PROTON DOSE ASSESSMENT TO THE HUMAN EYE USING MONTE CARLO N-PARTICLE TRANSPORT CODE (MCNPX)

A Thesis

by

DAVID BERNHARDT OERTLI

Submitted to the Office of Graduate Studies of
Texas A&M University
in partial fulfillment of the requirements for the degree of

MASTER OF SCIENCE

August 2006

Major Subject: Health Physics

PROTON DOSE ASSESSMENT TO THE HUMAN EYE USING MONTE CARLO N-PARTICLE TRANSPORT CODE (MCNPX)

A Thesis

by

DAVID BERNHARDT OERTLI

Submitted to the Office of Graduate Studies of
Texas A&M University
in partial fulfillment of the requirements for the degree of

MASTER OF SCIENCE

Approved by:

Chair of Committee,	John R. Ford
Committee Members,	John W. Poston, Sr.
	Michael Walker
Head of Department,	William E. Burchill

August 2006

Major Subject: Health Physics

ABSTRACT

Proton Dose Assessment to the Human Eye Using Monte Carlo N-Particle Transport Code (MCNPX). (August 2006)

David Bernhardt Oertli, B.S., Colorado State University

Chair of Advisory Committee: Dr. John R. Ford

The objective of this project was to develop a simple MCNPX model of the human eye to approximate dose delivered from proton therapy. The calculated dose included that due to proton interactions and secondary interactions, which included multiple coulombic energy scattering, elastic and inelastic scattering, and non-elastic nuclear reactions (i.e., the production of secondary particles). After benchmarking MCNPX with a known proton simulation, the proton therapy beam used at Laboratori Nazionali del Sud-INFN was modeled for simulation. A virtual water phantom was used and energy tallies were found to correspond with the direct measurements from the therapy beam in Italy. A simple eye model was constructed and combined with the proton beam to measure dose distributions. Two treatment simulations were considered. The first simulation was a typical treatment scenario—where dose was maximized to a tumor volume and minimized elsewhere. The second case was a worst case scenario to simulate a patient gazing directly into the treatment beam during therapy. Dose distributions for the typical treatment yielded what was expected, but the worst case scenario showed the bulk of dose deposited in the cornea and lens region. The study concluded that MCNPX is a capable platform for patient planning but laborious for programming multiple simulation configurations.

ACKNOWLEDGEMENTS

I would like to thank my graduate advisor, Dr. John Ford, for patience in answering my many questions and his unwavering support of my efforts. Special thanks to Dr. John W. Poston for his willingness to share his vast knowledge and experience in Health Physics, and a keen eye for editing. Thanks also to Dr. Walker for his insight, and efforts that made this project a success. Finally, and most importantly, special thanks to my family for their endless love and support—they are a constant catalyst for growth and an inspiration in love.

TABLE OF CONTENTS

Page

ABSTRACT …… iii

ACKNOWLEDGEMENTS..…… iv

LIST OF FIGURES …… vii

LIST OF TABLES …….. viii

CHAPTER

I INTRODUCTION AND BACKGROUND……..... 1

MCNPX Background……... 1
Proton vs. Conventional Radiotherapy...……. 4
Ocular Tumors……. 7
Ocular Tumor Treatments…..…….. 8

II MAKING OF A MODEL…….……... 12

Benchmarking …..……... 12
The Eye…… 18
Integrating the Eye and Beam…….. 20

III RESULTS AND DISCUSSION...……... 23

IV CONCLUSIONS….……. 33
Summary…….. 33
MCNPX Conclusions…….. 34
Eye Model Conclusions. ……. 36

REFERENCES …… 38

APPENDIX A…….. 43

APPENDIX B…….. 44

Page

APPENDIX C…….. 45

VITA…… 73

LIST OF FIGURES

FIGURE		Page
1	Typical photon IMRT planning and machine configuration……	5
2	Dose/depth comparison of photons vs. energy modulated protons……..	6
3	Uveal melanomas may include the iris (top left), choroid (top right)—and progress outward, or they may extend internally (bottom left)……	8
4	Heating mesh tally plot for a 200-MeV proton beam……...	13
5	Measured activity in water phantom and MCNPX simulation results...…..	15
6	Modulator wheels used with the Laboratori Nazionali del Sud-INFN proton beam……..	16
7	A spread out Bragg peak formed from the sum of individual Bragg peaks.	16
8	Measured Spread out Bragg peak (left), simulated (right)...……	18
9	MCNPX simulation of the human left eye……...	19
10	Typical proton treatment configuration……	22
11	Visual Editor illustration of the typical treatment geometry……	25
12	Dosimetric volumes in the eye model……..	26
13	Dose distribution for typical treatment case…….	28
14	Visual Editor illustration of the worst case geometry……..	29
15	Dose distribution for worst case scenario…….	31
16	Dimensions of the eye model……...	43

LIST OF TABLES

TABLE		Page
1	Interpretation of the relative error R……..……...	24
2	Dose distribution for typical treatment scenario……...	27
3	Dose distribution for worst case scenario…….	30
4	Dosimetric cell volumes……..	44

CHAPTER I

INTRODUCTION AND BACKGROUND

MCNPX Background

The Monte Carlo method describes a broad area of mathematics in which physical processes or other phenomena may be simulated using statistical methods through random numbers. One of the earliest examples of using random or chance events to ascertain truths hidden from common perception was demonstrated by Dr. de Buffon (Zaidi 2003). In 1777 he illustrated, by randomly tossing needles onto a table where parallel lines were drawn, that one could determine experimentally the value of pi. It was about 1944 when Ulam and von Neumann (Metropolis and Ulam 1949) coined the name 'Monte Carlo' during the World War II Manhattan Project. It was adopted from the well-known city in Monaco famous for its games of chance. Ulam and von Neumann led us into the modern age of Monte Carlo techniques and their application with modern computers was first realized in 1949, in simulations of neutron transport (Zaidi 2003).

Monte Carlo codes all follow the same general formulation. A model is created which is as similar as possible to the real system of interest, the model then is related to potential interactions within that system based on known probabilities of occurrence, by random sampling of probability density functions (pdfs). As more interactions occur within the simulation, the quality of the reported average behavior of the model improves, and therefore statistical uncertainty decreases. General components that are found in all Monte Carlo simulations include:

This thesis follows the style of Health Physics.

- Probability density functions: the physical system modeled must be related to reality through a described set of probability density functions.
- Random number generator: for uniformly distributing values on the unit interval.
- Sampling protocol: a prescribed method for sampling applicable probability density functions.
- Scoring: the outcome from the sampling must be tallied for quantities of interest.
- Error estimation: Statistical error (variance) must be calculated in light of the number of trials or other relevant quantities.
- Optimization techniques: methods for reducing the variance which also reduces required computational time.

The code MNCPX possesses all of these characteristics, serving as a general purpose Monte Carlo radiation transport code (Pelowitz 2005). It has progressed as a code to the point where it tracks nearly all particles and energies. It is the latest generation of transport code derived from 60 years of development at Los Alamos National Laboratory.

MCNPX development began in 1994 as program extension of MCNP4B and LAHET 2.8—with the goals of modeling all particles at all energies; improving physics models; extending of neutron, proton, and photonuclear libraries up to 150 MeV; and improving variance-reduction and data-analysis techniques (Pelowitz 2005). The program also incorporated cross-section measurements, benchmark experiments, deterministic code improvements, and better transmutation code and library tools.

The initial release of MCNPX occurred in October of 1997, and an extensive beta test team was formed to continually improve the code. Largely this team was driven by the feedback of MCNPX users. To date, approximately 1500 users in approximately 300 institutions around the world have had the opportunity to provide developer feedback. This process has tested MCNPX in a myriad of applications and conditions, proving it a useful and reliable tool. Applications for the code are broad and constantly increasing. Some examples include the following:

- Investigations for accelerator isotope production and destruction programs, including the transmutation of nuclear waste;
- Research into accelerator-driven energy sources;
- Investigations of cosmic-ray radiation backgrounds and shielding for high altitude aircraft and spacecraft;
- Accelerator-based imaging technology such as neutron and proton radiography;
- Design of shielding in accelerator facilities;
- Activation of accelerator components and surrounding groundwater and air;
- Investigation of fully coupled neutron and charged-particle transport for lower energy applications;
- Comparison of physics-based and table-based data;
- Charged-particle tracking in plasmas;
- Charged-particle propulsion concepts for spaceflight;
- Detection technology using charged particles (i.e., abandoned landmines);
- Nuclear safeguards;

- Radiation protection and shielding; and
- Medical physics, especially proton and neutron therapy.

The extensive testing, use, and constant improvement of MCNPX has yielded a reliable and useful tool for radiation transport computations. MCNPX has been widely recognized as capable of producing accurate and precise data for use in radiation patient treatment planning (Newhauser 2005). Simulations that were at one point thought to be incalculable have been resolved in reasonable simulation times through code improvements and increased computing power. Specifically, MCNPX can now take into account 3-dimensional geometry, coulombic energy loss, energy straggling, multiple coulomb scattering, elastic and inelastic scattering, and inelastic nuclear reactions (i.e., the production of secondary particles). The advances in Monte Carlo algorithms have led to the potential use in radiation treatment planning, however, until recently, attempts have not been made to demonstrate this capability (Newhauser 2005). Treatment planning with charged particles is an especially important area because of the intense local energy deposition.

Proton vs. Conventional Radiotherapy

Conventional radiotherapy, which applies photon beams, is the most frequently utilized modality for treating localized tumors. Tumor control is achieved through energy deposition from a high energy beam to a localized group of tumor cells. The challenge in radiotherapy has always been to maximize dose to the neoplastic growth, while minimizing radiation induced morbidity in surrounding healthy tissues.

In past years, photon therapy has progressed as a science, especially in the realm of imaging and treatment planning. To date the most advanced methodology is intensity-modulated radiation therapy (IMRT), which delivers higher doses to target cells as compared to dose delivered to surrounding normal cells. IMRT limits dose to healthy tissues by applying numerous radiation fields of varying intensities from different directions. Fig. 1 illustrates a typical photon IMRT assembly and patient planning.

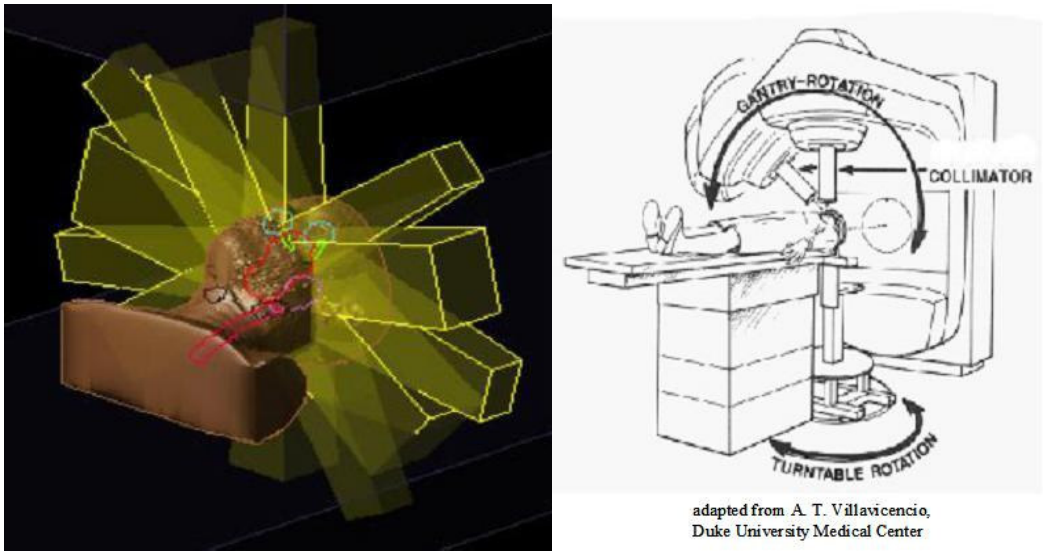

Fig 1: Typical photon IMRT planning and machine configuration (Liu 2005)

While IMRT reduces dose to healthy tissues, it requires a larger treatment volume—while energy deposition to the tumor area increases, it requires that more cells, over a greater area to be irradiated. This strategy significantly increases the integral dose to the patient. A concern for this type of treatment is the potential for secondary malignancies or other late tissue effects. This is especially a concern in pediatric patients—if such patients are cured of their primary malignancies, they are expected to have relatively

long lifespan during which radiation-induced effects might translate into health risks later in life.

In comparison to photon treatments, protons were recognized as having potentially superior dose distributions as early as 1946 (Wilson 1946). Protons, like all charged particles, exhibit a rapid energy loss at the end of their tracks. The resultant sharply localized peak of dose is known as the Bragg peak. The penetration depth of the Bragg peak is directly related to the initial energy of protons entering a target. The greater the initial energy, the deeper the occurrence of the Bragg peak. A comparison of a high energy photon beam and a modulated energy proton beam is shown in Fig. 2.

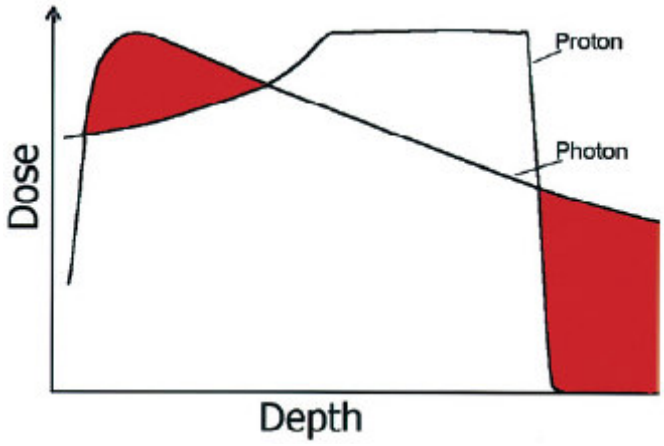

Fig 2: Dose/depth comparison of photons vs. energy modulated protons (Suit 2002)

In patient treatment, the peak energy deposition for protons is achieved by selecting a distribution of proton energies, where their combined Bragg peaks result in a uniform dose over the target volume. Instead of exhibiting a single Bragg peak, the peaks of various proton energies combine to give the cumulative effect of an extended Bragg peak, maximizing energy distribution across the patient target volume. This leads to superior dose in the target cells, but also minimizes exposure to healthy tissues beyond

the target. While photons will continue to deposit energy beyond the target volume, protons deposit all their energy in a small area—minimizing exposure beyond the target cells.

In some cases proton therapy has overwhelming advantages. Ocular tumors are an example. Eye function depends upon a number of tissues in close proximity. The cornea, lens, retina, fovea, and optic nerve are all critical organs for eyesight—radiotherapy can damage these organs leaving patients without eyesight. However, proton therapy in many cases has shown far superior results compared with photon treatments (Bertil et al. 2005). Proton treatment is often the first choice for pediatric patients. Since cured patients have potentially long life spans, radiation exposures are minimized to avoid potential radiation-induced risks later in life.

Ocular Tumors

Uveal melanoma and retinoblastoma are the principal tumors originating in the eyes of adults and children, respectively. Melanoma of the uveal tract is the most common primary intraocular cancer in humans—accounting for about 12% of all melanomas (Harbour 2003). Malignant melanomas appear most commonly in the choroid, followed in decreasing order by the ciliary body, the iris, the conjunctiva, and the skin of the eyelids. The rarest of the melanomas are those that originate from the cornea or the orbit. Incidence rates for these melanomas have been linked to genetic predisposition, immunological or hormonal alteration, and environmental and occupational factors, such as indoor working conditions, exposure to chemicals, radiofrequency radiation and ultraviolet light.

The appearance, size and location of uveal melanomas are highly variable, but clinical examination and ancillary testing can accurately diagnose most uveal and iris melanomas. This usually occurs through the use of ultrasonography because melanomas typically have lower reflective properties than surrounding tissues. Fluorescein angiography, magnetic resonance imaging, or fine needle aspiration biopsy are also possible diagnostic tools. Various tumors are illustrated in Fig. 3.

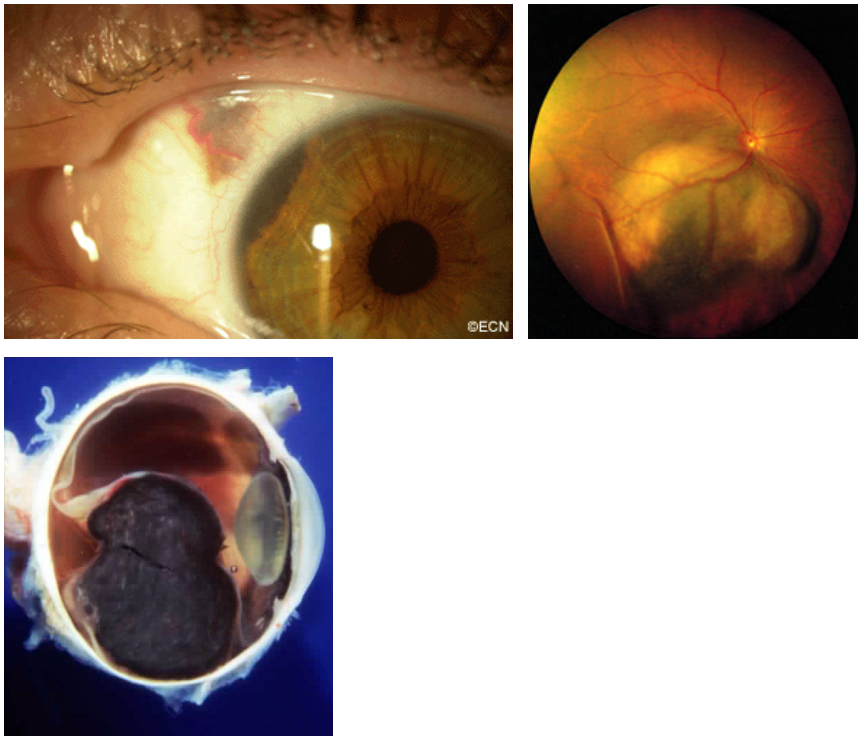

Fig 3: Uveal melanomas may include the iris (top left), choroid (top right)—and progress outward, or they may extend internally (bottom left). (Finger, Char, Kimmel Cancer Center 2006)

Ocular Tumor Treatments

To date the most common treatment for uveal melanomas is enucleation—removal of the entire eyeball. This is most considered mostly in cases that involve:

- Large tumor size;
- Tumor invasion of the optic nerve head;
- Lack of access for other treatment options;
- Inability to return for follow-up; and
- Patient choice.

In the 1970s, Zimmerman and his colleagues were the first to document the phenomena that enucleation actually has the potential to speed metastatic progression (Zimmerman et al. 1978). This may occur because additional tumor cells are released into the bloodstream during the handling of the eye in the enucleation process. It has also been observed in animals that primary tumors may produce angiostatin, a tumor suppressant that effectively inhibits angiogenesis and additional metastatic growth. This study which has been repeated many times, leads some to the conclusion that in-place treatment is preferable when possible.

Perhaps slightly more conservative than enucleation is local resection within the eye. When a patient must retain vision in a seeing eye, or the tumor cells are in the only remaining eye, local resection might be a desired approach. This procedure entails surrounding the area of resection with photocoagulation barrages over several weeks to cut off the choroidal blood supply to the area. The portion of the sclera, choroid, or retina with the tumor is then excised, and the wall defect is repaired with a sclearal graft. This is a complicated surgical procedure, which has a high probability for seeding tumor cells into the wound or outside the eyeball (Albert and Polans 2003).

Transpupillary Thermotherapy was developed as a less evasive method for treating intraocular tumors. The most current treatments are applied using an infrared diode laser

(projecting a spot size of 2-3 mm), used for about 1 minute per exposure. The laser heats lesions to a temperature great enough to induce necrosis without photocoagulation in target cells. Limitations of this treatment include depth of treatment at 3.9 mm, potential for unfavorable side-effects such as macular traction, retinal vascular occlusion, macular edema, retinal or vitreous hemorrhage, and visual field defects. Thermotherapy is usually applied concurrently with some form of radiotherapy (Godfrey 1999).

Radiotherapy is typically applied in one of three forms: conventional external-beam, brachytherapy, and charged particles. Conventional external-beam therapy is available, but generally not applied due to complications discussed previously. Brachytherapy is a more recent development aimed at delivering localized radiation with fewer side effects than external beam therapy. A typical configuration involves attaching radioactive seeds to a lead or gold "plaque" that is sewn to the sclera overlying the imbedded tumor. Common radionuclides include iodine-125, ruthenium-106, and palladium-103. Typically 80-100 Gy is delivered to the tumor apex over a 4-5 day period, with a 2-mm margin around the tumor base (Robertson 1983). Limitations include the invasive nature of treatment, and radiation side-effects including: cataracts, retinopathy, papillopathy, and neovascular glaucoma. These effects are strongly dose-dependent and begin to increase sharply at 40 Gy (Parsons 1996), which is below the minimum level needed for local tumor control.

As discussed previously, charged particle therapy is a means for delivering highly focused radiation to tumor areas. This is arguably one of the best options for treatment. Zimmerman and his co-workers (Zimmerman et al. 1978) identified an important trend

in metastatic progression following invasive treatments. Enucleation and local resection are the only treatment options that introduce the risk factor that tumor cells may seed in other tissues as a result of the invasive handling of lesions. Brachytherapy, or the use of radiotherapy plaques, is also fairly invasive and introduces surgical difficulties that affect accuracy of plaque placement. Thermotherapy is less invasive, but not as effective. The limited depth of treatment is a significant shortcoming, and it requires concurrent treatment with other modalities. Charged particle therapy, or specifically proton therapy does have limitations—it can be cost prohibitive, it has higher potential for anterior segment complications, and neovascular glaucoma occurrence is higher than in other treatments. However, proton therapy boasts superior tumor control after treatment compared with other radiotherapy methods, which greatly lowers the risk of metastic disease. The non-invasive nature of treatment is also a positive aspect of proton therapy. Less manipulation of the eye translates into less potential for unintended spreading of tumor cells, and accidental changes in position of the treatment target volume. In spite of the limitations, proton therapy is now a leading treatment modality for ocular tumors (Levin et al 2005).

CHAPTER II

MAKING OF A MODEL

Benchmarking

To establish that the MCNPX code was functioning as expected, a known simulation was applied locally. A 10-cm diameter 200-MeV proton beam was constructed to irradiate a cylindrical water phantom. Three smaller cylinders were placed in the path of the beam (inside the water phantom) to test the qualitative interactions with the proton beam. The first cylinder was defined as a zero-importance area for protons—meaning that any protons that enter the volume ceased to exist. The second cylinder in the path of the beam was constructed of iron, and the third was defined as a void space. Qualitatively speaking, one would expect that particles would cease to exist in the zero-importance area, and that a "shadow" would be observable down-stream of the source from that volume. In the iron cylinder one would expect greater interaction corresponding to a much higher proton stopping-power and short proton path length. Finally, in the void volume, we would expect to see no interactions—and a greater path length for particles downstream of the void (due to a decrease in particle interactions in their path of travel due to the void).

To illustrate the results of this benchmark, a mesh tally plot was used. Mesh tallies were used for tracking fluxes, heating, source locations, doses and other tally quantities. For this case, a heating mesh tally was applied and plotted. The results are shown in Fig. 4.

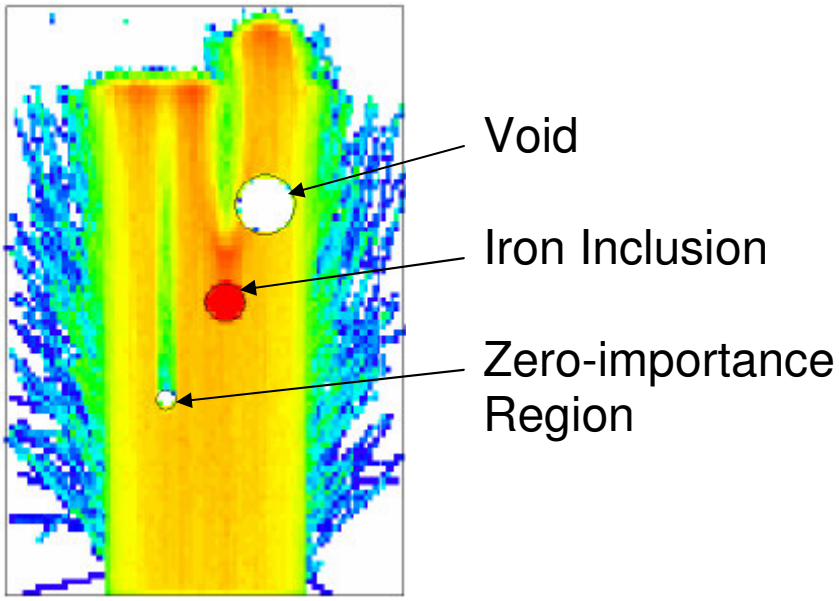

Fig 4: Heating mesh tally plot for a 200-MeV proton beam

Results of the 2-D plot of the water phantom with inclusions yielded what one would expect. The blue color scheme indicated cooler regions, while the red showed higher temperatures. The zero-importance area (far left inclusion) indicated desired qualitative results. Very limited interactions were found inside the volume (zero-importance was applied to protons, not all particles). There was also an abrupt change in proton interactions downstream of the zero-importance area as evidenced by a clear shadow following the zero-importance volume. The iron inclusion showed greater heating as expected, and downstream from the iron inclusion, the length of travel for protons was much less than what was found elsewhere. The last inclusion, a void, also yielded the expected results. There were no interactions in the void, and there was clearly a longer path of travel for protons that traveled downstream from the void. A flux tally was also plotted and appropriate values were obtained. These tests confirmed that the MCNPX code was simulating the proton beam at least qualitatively.

To benchmark a beam for radiotherapy simulation, the proton therapy beam used at Laboratori Nazionali del Sud-INFN was selected as a model for the simulation. Built in collaboration with the University of Catania (Italy), the 62-MeV proton beam is used for treatment of ocular pathologies like uveal melanomas, choroidal hemangiomas, conjunctiva melanoma, eyelid tumors, and embryonal sarcomas. Before each treatment, the beam is calibrated using a water phantom with embedded PTW 34045 Markus Ionization Chambers. The ion-chambers have an electrode spacing of 1mm and sensitive air-volume of 0.02 cm^3. Dose measurements using the phantom and embedded ion-chambers have been compiled and published (Cirrone 2004).

To simulate the 62-MeV beam, the original MCNPX simulation source energy and beam diameter were adjusted to match the Laboratori Nazionali del Sud-INFN proton beam. The MCNPX water phantom was subdivided into progressive layers of water in which deposited dose was tallied. This enabled measurement of energy deposition as a function of depth in the phantom. The simulation yielded the expected Bragg peak behavior. The maximum penetration depth is slightly greater in the simulation. This is primarily due to electron straggling effects, and lower energy cut-off in simulation. The MCNPX code does not track scattered electrons with an energy value lower than 1 keV. This approximation eliminates some of the dose due to delta-rays in the target. Likewise the lower-energy cut-off for protons is 1 MeV, which lowers the overall dose in the target and explains the slight variation between the two sets of data. Measured values obtained in Italy and the MCNPX simulation results can be compared in Fig 5.

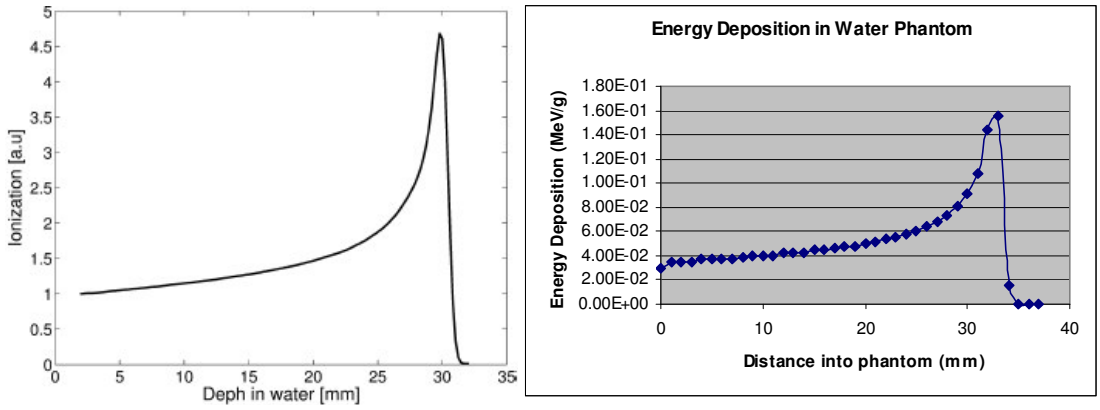

Fig 5: Measured activity in water phantom (left), MCNPX simulation results (right)

For applying treatment to individuals, it is common practice to introduce a modulating device and a range shifter to effectively spread out the Bragg peak and vary the maximum distance of the beam. The modulator acts on the beam to effectively vary the beam energy such that a carefully selected spectrum of proton energies emerge so that a uniform dose over the volume of interest will result. This is usually achieved by placing a spinning disk, or a modulator wheel, between the source and target. The spinning wheel has different material characteristics at different points on the disk. As the proton beam interacts with the modulator material, beam characteristics are changed, creating a spectrum of proton outputs. Fig. 6 is a photo of a modulator wheel used in proton therapy at Laboratori Nazionali del Sud-INFN.

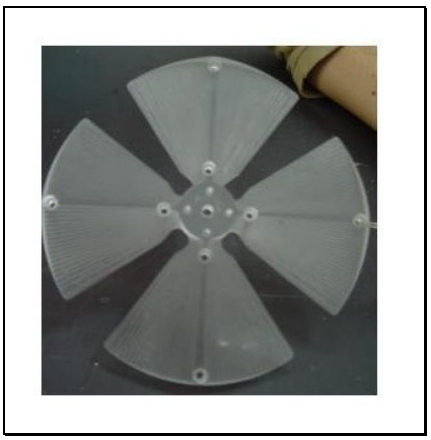

Fig 6: Modulator wheels used with the Laboratori Nazionali del Sud-INFN proton beam (Cirrone 2005)

If one sums together the various Bragg peaks of individual proton energies exiting a modulation wheel, a spread out Bragg peak can be obtained, as illustrated in Fig. 7.

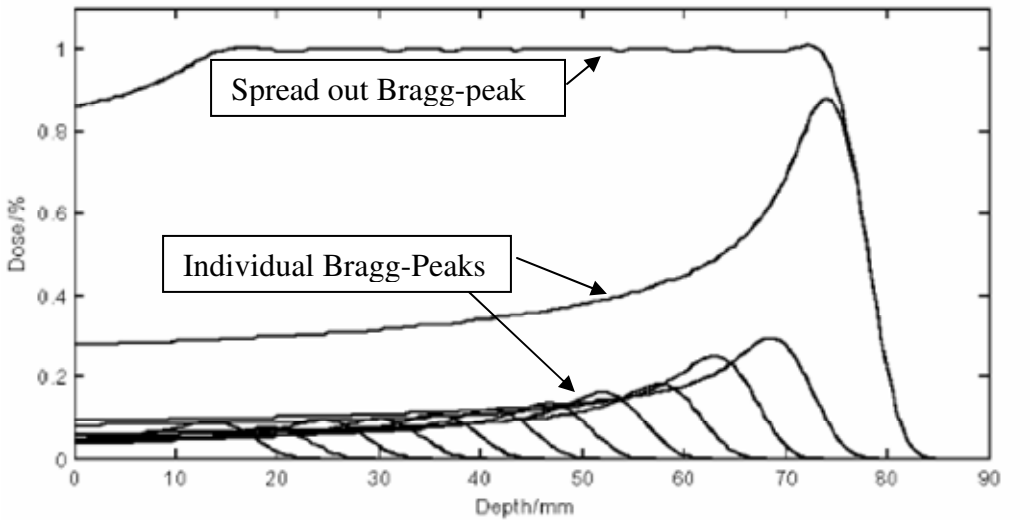

Fig 7: A spread out Bragg peak formed from the sum of individual Bragg peaks (Kooy 2003)

The resultant beam deposits much higher energies over a larger target volume. This allows high-energy treatment to a tumor volume instead of a tumor point, and at the same time minimizes dose beyond the tumor cells.

To model a modulator wheel in MCNPX is a challenging task. A limitation of most Monte Carlo simulations (MCNPX included) is that material properties cannot vary with time during a simulation. To model a rotational wheel in the geometry of a simulation is impossible. A varying source however is possible, but to find the energy spectrum necessary for the spread out Bragg peak is a not trivial.

The MCNPX code is able to vary energy emitted from a source if an energy spectrum is defined, and each energy level is weighted as to how often it is emitted. Trial and error was the first method for finding an appropriate spectrum, but this was quickly abandoned because of the complexities involved. To obtain precise data points, a MATLAB routine was made that incorporated the original 62-MeV MCNPX Bragg peak data. The MATLAB routine combined lower energy protons into the spectrum and the frequency with which each should be introduced into the beam for the desired effect. The result was a spread out Bragg peak that closely simulated the actual data collected from the Laboratori Nazionali del Sud-INFN proton beam. As previously discussed, slight variations between the two can be attributed to lower energy cut-off for protons energies less than 1 MeV and electrons less than 1 keV. A comparison of the two outputs can be seen in Fig. 8.

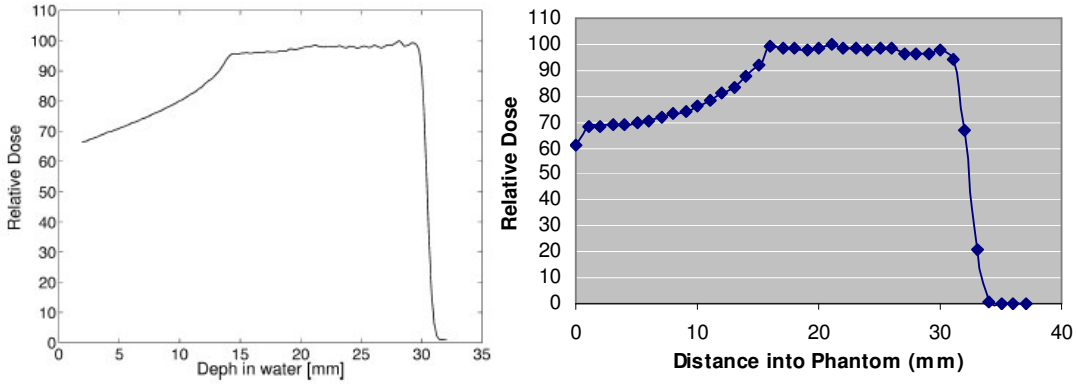

Fig 8: Measured Spread out Bragg peak (left), simulated (right)

With this, the MCNPX simulation had been appropriately benchmarked. A known simulation was used to find expected output—the simulated water phantom with tally inclusions calculated results as expected. After selecting the Laboratori Nazionali del Sud-INFN proton beam for a therapy simulation, the previous MCNPX model characteristics were adjusted. The energy level and beam diameter were set to match conditions used with the Laboratori Nazionali del Sud-INFN beam. Dose distribution into the water phantom was verified with actual data, and a spread out Bragg peak from the simulation matched closely the actual proton beam characteristics.

The Eye

One of the potential benefits of proton therapy is that ocular tumors can potentially be treated in-place, avoiding more evasive procedures like local resection or enucleation. Preserving eyesight through the course of in-place treatment is a challenging task because the critical organs necessary for eyesight are located so closely together. These critical organs for eyesight were the emphasis of the MCNPX model. The lens of the eye has long been understood to be a radiosensitive organ. Likewise, radiation exposure

to the cornea can cause the structure to become opaque and obstruct vision. Since many uveal melanomas appear in the choroid and sclera structures of the eye, these needed to be modeled. Lastly, the optic nerve bundle near the posterior axis of the eye was an area of interest. A two dimensional rendering of the eye used for the MCNPX modeling is shown in Fig. 9.

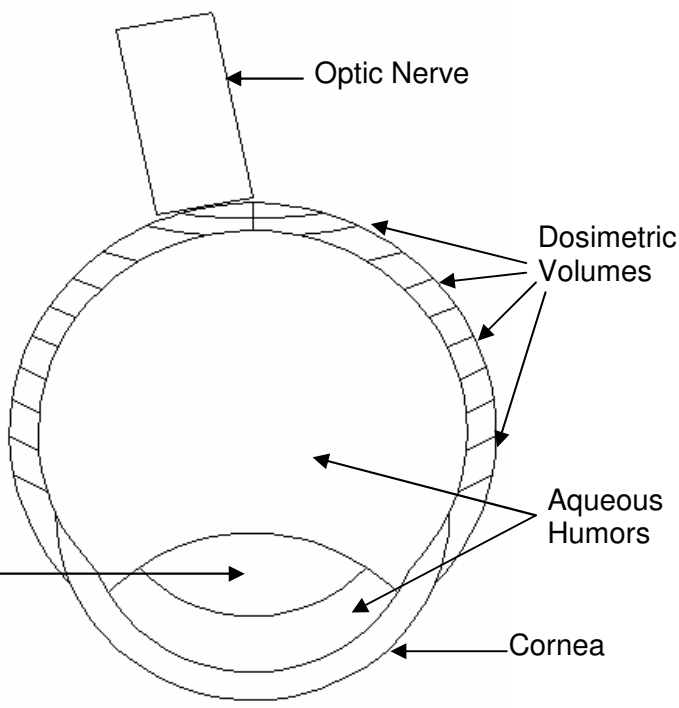

Fig 9: MCNPX simulation of the human left eye

Dimensions of the human eye were adapted from *Optics of the Human Eye* (Atchison and Smith 2003). The model was constructed using concentric spheres, offset as appropriate. The vitreous humor was defined to be the volume posterior to the lens, and the anterior chamber, anterior to the lens. The delineation is marked in Fig. 9 by lines from the ends of the lens to the cornea. The optic nerve is simulated as a cylinder appropriately offset from the posterior pole of the eye. The subdivisions in the outer wall of the model are volumes for dosimetric tallies.

Material compositions for the model were adapted from the International Commission on Radiation Units and Measurements (ICRU) Report 46, *Photon Electron, Proton and Neutron Interaction Data for Body Tissues*. This report addressed various tissues groups in the body and defined their elemental composition and densities for purposes of radiation dosimetry. The lens of the eye is addressed directly in the publication; however the other components of the eye were approximated. Recent studies have indicated the vitreous and anterior humors have characteristics similar to the properties of lymph outlined in ICRU 46 (Macknight 2000 and Brzezinski 2004). The choroid and sclera are essentially connective soft tissue and were modeled correspondingly as soft tissue. The optic nerve was approximated using the elemental composition of nerve tissue in rats (Stys and Lopachin 1996).

Integrating the Eye and Beam

With the eye modeled and the proton beam simulation benchmarked, the next step was to combine the two together in a realistic way. The positioning of the target relative to the therapy beam is of course vital in treatment of any tumor. For treatment of patients with proton therapy, this is typically achieved through a series of appointments at the treatment facility. Following the diagnosis of a tumor, the size and dimensions are identified relative to other parts of the eye. The shape and location of the tumor are then marked by an ophthalmologist using tantalum marker clips which are sewn to the outside of the sclera. The shape and position of the target volume are outlined by the clips. This form of marking a target area is noninvasive enough that the clips are generally not removed from the patient following treatment.

One to two weeks after the insertion of surgical clips, the patient returns to the treatment facility to establish the position of the head needed for the proton treatment. Two main tools are used to immobilize the patient's head, a custom block-bite and individual mask. The block-bite is a piece of material the patient bites down on during the treatment. It is custom made to fit the individual patient's teeth, ensuring consistent placement in the patient's mouth as they bite down on the block. Likewise, the individual mask is a form-fitting mesh that fits over the individual's face and is anchored behind the head. The mask is set firmly against the patients face and head, then anchored to ensure immobilization. The combination of the block-bite and custom mask allow precise and accurate placement of the patient relative to the beam. One treatment facility reports reproducibility of 1/10 mm along 3 linear axes and 2 rotational axes (Heufelder 2006). Once the patient has been effectively immobilized in a reproducible position, a series of diagnostic x-rays are taken to precisely measure the positions of the marker clips in the eye relative to the patients' position and the treatment beam.

With the geometry of the head relative to the beam established, the treatment team reviews diagnostic images (MRIs, CTs, sonograms, patient placement x-rays) and plans the proton target dose and the necessary angle of the eye for treatment. To fix the gaze of the patient at the appropriate angle, a small light or other focal point is moved into a position where the patient can focus their gaze to an exact point. The angle of the patient's gaze can help to minimize the dose to critical organs. For example, in treatment of a posterior melanoma, it may be possible for the patient to fix their gaze looking toward the ceiling, effectively moving the cornea and lens out of the proton

treatment path. After combining all the information together with a therapy plan, a feasibility check is done and the patient is ready for treatment. A typical treatment configuration is shown in Fig. 10.

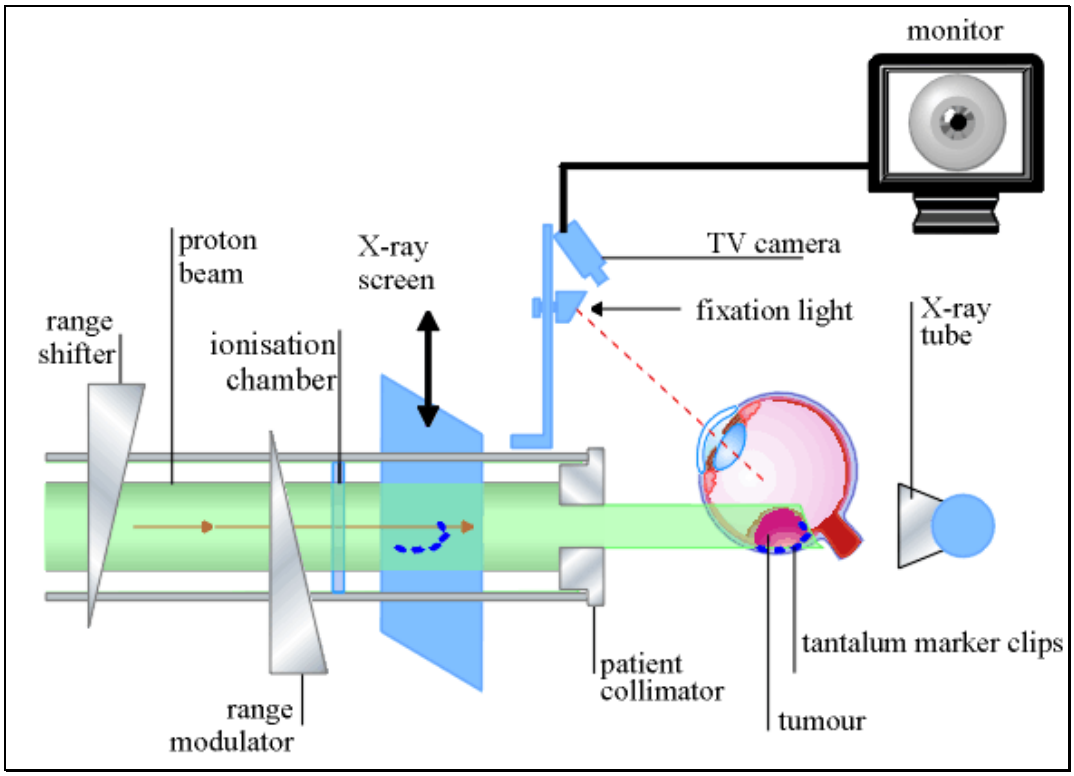

Fig 10: Typical proton treatment configuration (Heufelder 2006)

To combine the eye and the beam to a similar configuration for the MCNPX simulation, two cases were considered. The first was a typical treatment scenario, with the intent was to irradiate a tumor area at the posterior of the eye with minimal effect to critical organs of the eye. The second was a worst case scenario, where the patient's gaze changes to place the cornea and lens directly into the path of the beam.

CHAPTER III

RESULTS AND DISCUSSION

Two cases were taken for proton radiotherapy simulation. The first, a typical scenario where exposure to the eye was minimized and a potential tumor volume was exposed to maximum proton dose. The cancer simulation was a uveal melanoma in either the choroid or sclera of the eye. The second case was a worst case scenario in which the patient changed their gaze to look directly into the proton beam—maximizing dose to the cornea and lens.

Just as with a patient proton beam treatment configuration, beam adjustments in the simulation needed to be made to contour the beam to the treatment volume. Two modifications were necessary to contour the beam appropriately. A range modifier was introduced to adjust the maximum penetration depth of protons from the beam, and a modulator to change the energy spectrum creating a spread of the Bragg-peak over the appropriate target volume. A range modifier of water was modeled between the proton source and the eye, lowering the maximum distance traveled by individual protons, and limiting delivered dose outside the target volume. Likewise a modulator wheel was simulated to spread out the Bragg-peak, effectively distributing proton dose over the target volume. The same spread out Bragg peak simulated in the proton beam benchmark was used for the therapy simulations.

At first, the eye model was used with all material properties set to water. This allowed output data to be compared qualitatively with the benchmark data in the water phantom. Results yielded dose distributions and proton penetration depths that were consistent with the benchmarked results.

Next the materials of the eye were changed to material compositions that more closely matched the actual composition of the eye and a calculation was made for typical patient treatment scenario. For this typical treatment scenario, the proton beam was positioned to give minimal dose to the lens and cornea. The majority of the proton dose was deposited in the choroid/sclera and vital organs for eyesight were largely spared.

To ensure the precision of these results, the MCNPX code includes ten standard statistical indices. All of the proton beam simulations earned passing marks. Two of the indices are discussed here. First, the tally mean measured fluctuation of tally counts in relation to fluctuation in the number of particles simulated. There should be only random fluctuations in tally values with increased particle histories, which was the case with the proton beam simulations. Another statistical measure is the relative error (R). This is perhaps the most scrutinized of the statistical indices. It relates the tally mean with the overall uncertainty—specifically it is the ratio of the standard deviation of the tally mean to the overall mean. R is typically interpreted against the criteria shown in Table 1 (Shultis and Faw 2006).

Table 1. Interpretation of the relative error R.

Simulation R Value	Quality of Talley
> 0.5	Meaningless
0.2 to 0.5	Factor of a few
< 0.1	Reliable (except for point/ring detectors)
< 0.05	Reliable even for point/ring detectors

The relative error for the typical treatment scenario and the worst case scenario were 0.008 and 0.0012, respectively—reflecting extremely low relative error. After numerous

simulations it was clear that following 300,000 histories was sufficient to obtain excellent statistics. As an added precaution, these calculations were made several times to ensure similar results. In addition to tally mean and relative error, 300,000 particles simulations attained excellent statistics in the remaining eight statistical indices in MCNPX.

To obtain a graphical representation of what was occurring, MCNP Visual Editor Version 12N was used. The MCNPX input file was loaded in Visual Editor to illustrate the geometry of the problem. In Fig. 11, the treatment beam travels through a water range modifier and is incident on the outer structure of the eye. Arrows have been added to indicate the path traveled by the proton beam.

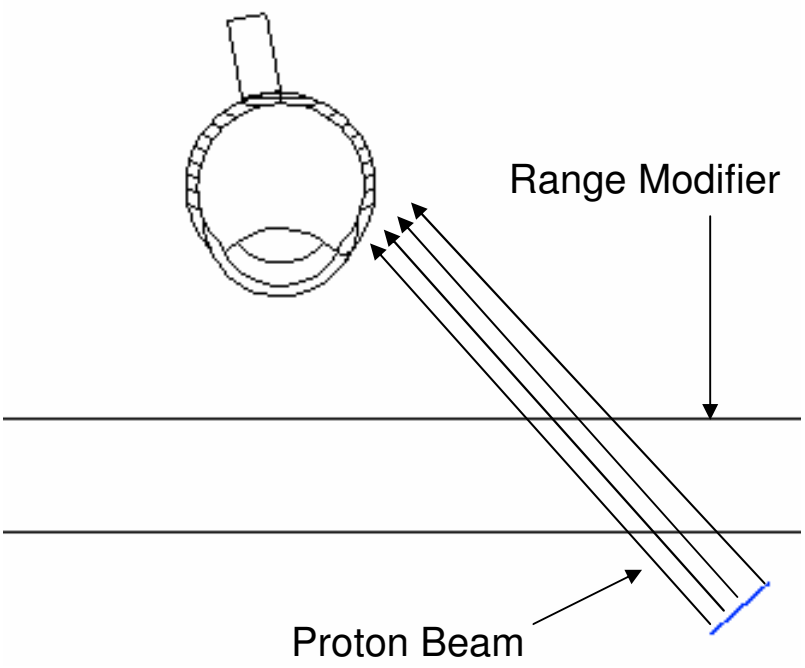

Fig 11: Visual Editor illustration of the typical treatment geometry

To obtain the delivered dose to various parts of the eye, the model was subdivided into dosimetric volumes, which include the lens, cornea, anterior and vitreous humors, and a series of volumes in the wall of the eye (see Appendix A). These volumes are illustrated in Fig. 12.

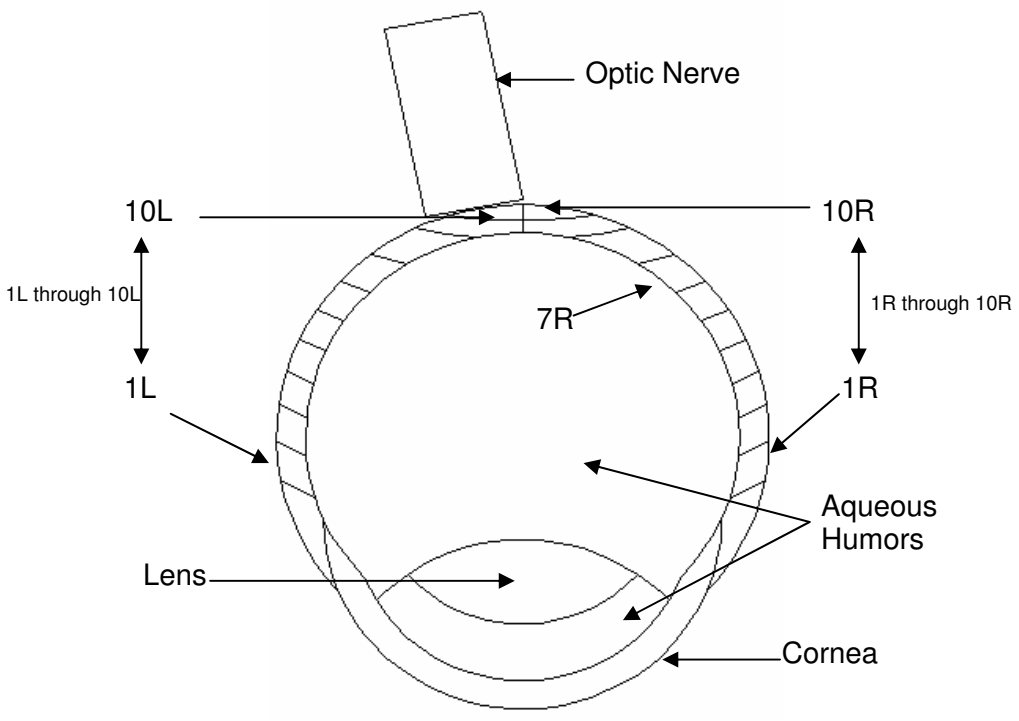

Fig 12: Dosimetric volumes in the eye model

For the typical treatment scenario the volume 7R was identified to contain the cancerous tumor. The simulation was run to maximize dose to this portion of the eye, and minimize it elsewhere. The results for the typical treatment scenario are found in Table 2.

Table 2. Dose distribution for typical treatment scenario

Dose Volume	Dose per Fraction (Gy)	Total Dose (Gy)
Cornea	0.60	2.41
Anterior humor	0.09	0.37
Lens	0.09	0.36
Vitreous humor	4.93	19.73
Optic Nerve	1.06	4.26
1R	11.01	44.02
2R	10.86	43.45
3R	10.25	40.99
4R	9.71	38.85
5R	9.67	38.70
6R	10.51	42.02
7R	12.50	50.01
8R	10.22	40.89
9R	1.56	6.23
10R	0.02	0.09
1L	0.02	0.06
2L	0.01	0.04
3L	0.01	0.03
4L	0.00	0.01
5R	0.00	0.00
6L	0.00	0.00
7L	0.00	0.00
8L	0.00	0.00
9L	0.00	0.00
10L	0.00	0.00

A typical proton therapeutic dose for uveal melanoma in this portion of the eye is about 50 Gy spread over four fractions, which translates into four treatments of 12.5 Gy delivered to the patient (Heufelder 2006). To match this treatment as seen in Table 2, the simulation was optimized to maximize dose to 7R (12.5 Gy per fraction, 50.01 Gy overall) while minimizing dose elsewhere. The left side of the eye received doses at least three orders of magnitude lower than those of the right side. The optic nerve was a concern, not because the tissue is as radiosensitive, but because it was directly in the path of the proton beam. Results showed however, that dose to the optic nerve was

relatively small—only about 1 Gy per fraction. This is within acceptable the limit of 10 Gy to the optic nerve for treatment with protons (Jones and Errington 2000). For each treatment the cornea received less than 3 Gy, well within the acceptable limit of 15 Gy (Simonva 2002). For the lens of the eye, special effort is made in therapy to keep doses at an acceptable limit—typically less than 8 Gy (Jones and Errington 2000). In this simulation, cumulative dose to the lens of the eye from the 4 fractions was only 0.36 Gy, while the dose to the target volume was over 50 Gy. The dose distribution is shown graphically in Fig 13.

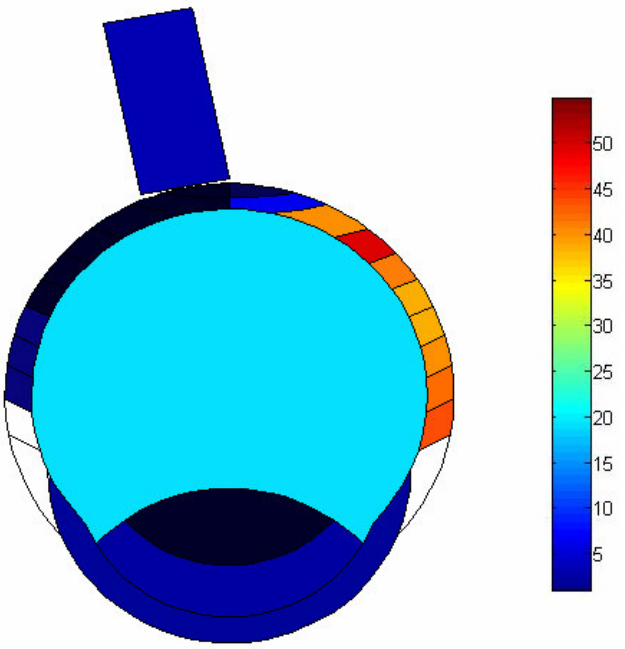

Fig 13: Dose distribution for typical treatment case

For the worst case scenario, the beam was situated to treat the same cancerous target volume, with the lens of the eye in the path of the beam. Since the object of this simulation was to mimic a patient gazing into the beam during treatment, the same dose

profile from the typical treatment scenario was used. The geometry for this simulation was illustrated using Visual Editor and arrows were drawn in to represent the proton beam. A water range modifier can also be seen at the bottom of Fig. 14.

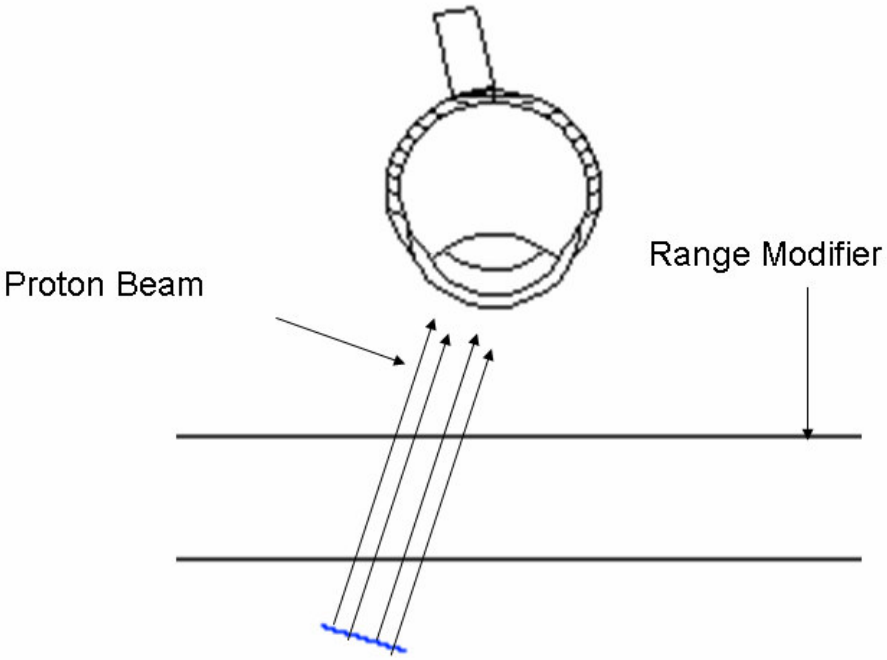

Fig 14: Visual Editor illustration of the worst case geometry

The results from the worst case simulation are shown in Table 3.

Table 3. Dose distribution for worst case scenario

Dose Volume	Dose per Fraction (Gy)	Total Dose (Gy)
Cornea	9.02	36.08
Anterior humor	25.38	101.52
Lens	38.72	154.89
Vitreous humor	5.96	23.84
Optic Nerve	0.00	0.00
1R	0.16	0.64
2R	0.14	0.57
3R	0.09	0.37
4R	0.01	0.05
5R	0.00	0.01
6R	0.00	0.00
7R	0.00	0.00
8R	0.00	0.00
9R	0.00	0.00
10R	0.00	0.00
1L	0.11	0.42
2L	0.09	0.35
3L	0.07	0.28
4L	0.06	0.25
5R	0.05	0.21
6L	0.03	0.14
7L	0.00	0.02
8L	0.00	0.00
9L	0.00	0.00
10L	0.00	0.00

Surprisingly, the dose to the cancerous volume in the eye is zero for this configuration. The majority of the proton energy is deposited within the cornea, anterior chamber and lens of the eye. If one fraction of therapy was conducted in this manner, just over 9 Gy would be delivered to the cornea and, if this configuration occurred for the duration of treatment, the patient would experience over 36 Gy to the cornea. One would expect a detrimental effect to the cornea at a threshold of about 15 Gy (Simonova

2002). With such a high dose, one might observe keratitis and corneal ulcerations possibly leading to perforation of the cornea. Likewise, the lens incurred high doses. For a single fraction in this position, 38.7 Gy would be delivered to the lens. For the treatment series, the total lens dose would be 155 Gy, compared to the accepted tolerable dose of 8 Gy (Jones and Errington 2000). One would expect severe visual loss due to the lens becoming opaque in this treatment scenario. The cumulative dose in the tumor volume for this configuration is zero, which is illustrated in Fig 15.

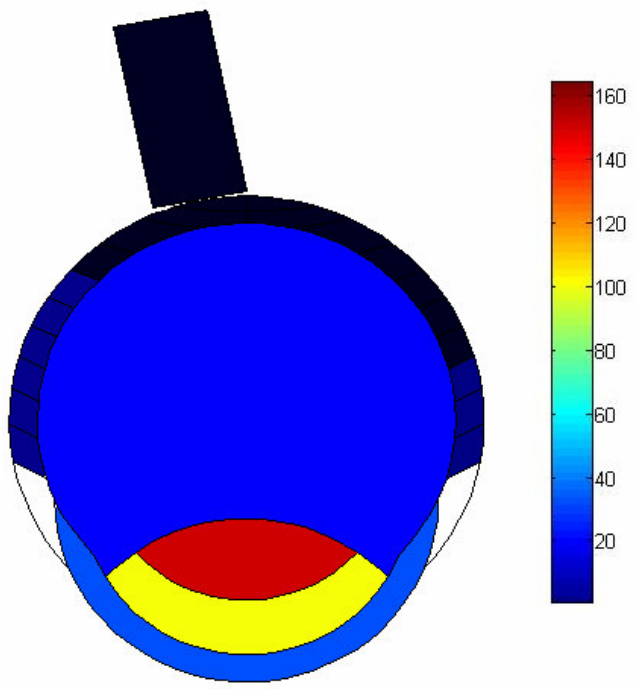

Fig 15: Dose distribution for worst case scenario

The data from the worst case may be the most useful of the simulation data. Published data are virtually nonexistent for a worst case scenario like this. Of course there are minimal human *in vivo* data for dose reconstruction of this type—this simulation gives an approximation that could be used to reconstruct dose following an

accident in treatment. If a patient was to alter their gaze directly into the treatment beam, one could reconstruct the dose by the fractions of time in each treatment position. The fractions of dose from each position would translate to dose delivered to the lens and cornea, and dose lost from the target volume.

CHAPTER IV

CONCLUSIONS

Summary

The primary objective of this project was to develop a model of the human eye using the computer code MCNPX that approximates dose delivered during proton therapy. The calculations considered proton interactions and secondary interactions, which included multiple-coulombic-energy scattering, elastic and inelastic scattering, and non-elastic nuclear reactions (i.e., the production of secondary particles). After benchmarking the MCNPX code with a known proton simulation, the proton therapy beam at Laboratori Nazionali del Sud-INFN was modeled for simulation. A virtual water phantom was used and energy tallies corresponded with the direct measurements from the therapy beam in Italy. An eye model was created and combined with the simulated proton beam. Dose was tallied for two specific treatment cases; first, a typical treatment case where dose to the tumor was maximized, while doses to critical organs for eyesight were minimized. The second case was a simulation where the patient gazed directly into the beam during treatment. Doses for both cases were calculated throughout the eye: the lens, cornea, anterior and vitreous humors, optic nerve, and a series of volumes in the wall of the eye.

Results for a typical treatment scenario yielded the desired outcome. The dose to the tumor volume was at therapeutic levels and, at the same time, doses to the cornea, lens and optic nerve were well within acceptable limits. For the worst case scenario, the result was a large dose to the cornea, lens, and aqueous humors. The tumor did not receive any dose in this configuration.

MCNPX Conclusions

The premise for this endeavor was that the MCNPX code is a capable platform, largely under-utilized for this type of application. While true, there maybe some reasons for its scarce use in the past, e.g., the complexity of data input and limited flexibility in geometry and treatment modifications. The user interface for the MCNPX code is simply line by line coding—an interface updated little with the progression of technology in past years. Other programming languages have progressed to more user friendly interfaces; like Visual Basic or Visual C++, characterized by mouse controlled graphics, drag-and-drop icons, and common code progressions that can be duplicated and inserted into new programs. Input into the MCNPX code in comparison is laborious and antiquated. During the construction of the eye model, changes in geometry were made that propagated errors throughout the rest of the code. A single change in geometry necessitated careful inspection of cell definitions, tally boundaries and volumes. One change might require careful inspection of three or four sections of the code to ensure all variables were still correctly defined and compatible. If errors were still present in the edited code, the error messages generated were often unable to identify the specific error, but instead indicated the need for line by line analysis to restore the simulation function. Worse yet, there were a handful of potential errors that did not generate error messages. In some cases, the simulation was conducted with obvious errors and produced erroneous output. Many of the inconveniences that make the MCNPX code difficult to use could be potentially engineered out by redesigning the user interface. If the input was a graphical interface, with coding as a secondary method of input, the efficiency of data input could sky-rocket. To draw the simulated eye-model

in a CAD program would take a few hours and, if cells, tally points and volumes mirrored a graphical rendering, it would eliminate the need to scrutinize many sections of code after making one minor change. While the MCNP Visual Editor is an attempt at a graphical interface, and has proven itself a wonderful tool for verifying geometry, there is still much to be desired in the program. The inflexibility of the current MCNPX code might easily translate into lost time in dose planning and overall treatment time in a medical facility. The usefulness of the current laborious interface might be questionable for day-to-day practice in a treatment facility.

On a positive note, the MCNPX code performed surprisingly well once the program was working correctly. The simulation run times ranged from 10-13 minutes. In that time range the MCNPX statistical indices yielded outstanding results. The relative error was extremely low for the typical and worst case scenarios—0.008 and 0.0012, respectively. Likewise, all the others statistical indicators resulted in values far beyond the threshold for credible results. This provided assurance that once the geometry, cells, and tallies were input, errors in the code were identified and corrected, one can expect very precise results.

The MCNPX code also has additional helpful features that could be incorporated into future proton beam simulations. For example, MCNPX Version 2.5.0 features mesh tally plots which apply to fluxes, heating, doses or other tally quantities plotted on a 3-D mesh surface (rectangular, cylindrical, or spherical) independent of the problem geometry. This could be used to graphically illustrate tissue heating effects due to proton treatment, or doses over the volumes in, or adjacent to the eye. The propagation of heat, dose, or other tally values might be a fruitful study for tumors near sensitive

organs such as the optic nerve—while flux values taken over the eye might more clearly define scattering effects and adjacent dose distribution during treatment.

Eye Model Conclusions

Greater detail could be incorporated into the current model of the eye—effectively expanding the types of cancerous tumors which might be modeled. Regions outside the eye were neglected in the creation of this model. Adjacent organ dose is inferred by adjusting the penetration depth of the beam with a range modifier, and confirming the dose by Bragg peak behavior in the tallies. This may not be an adequate in all cases. The boney structure of the skull for example, could be a limiting factor in treatment angles of the proton beam—if the treatment angle is too great, the bone protruding from below or above the eye socket might interfere with treatment. Likewise, the soft tissues surrounding the eye will receive dose when the beam is placed outside transpupillary treatment angles. Adding these structures would lead to better understanding of doses outside the eye, and potential limitations of treatment angles.

Inside the eye, greater accuracy could also be attained by adding more detail. For example the cilliary bodies and the iris surrounding the lens are areas where cancerous growth can occur. With the current eye model it was not be possible to simulate these types of tumors and their treatments. Likewise, greater resolution could be obtained by differentiating between organs located closely together in the eye, like the sclera, choroid, and the retina. For purposes of the typical treatment and worst case scenarios, combining them into a general outer structure of the eye was sufficient, but

differentiating might be helpful for studying treatment scenarios for a range of tumors at various stages of progression.

REFERENCES

Albert D, Polans A. Ocular Oncology, New York: Marcel Dekker; 2003

Atchison D, Smith G. Optics of the Human Eye, Edinburgh: Reed Educational and Professional Publishing; 2003.

Bertil D, Ophth FRC, Kacperek A, Chopra M, Campbell I, Errington RD. Proton beam radiotherapy of choroidal melanoma: the Liverpool-Clatterbridge experience. Int J Radiat Oncol Biol Phys 62(5):1405-11; 2005.

Brzezinski P, Godlewski A. Assessment of potassium and sodium ion concentrations in the vitreous humour of swine isolated eyeballs after organism death. Rocz Akad Med Bialymst 49:161-3; 2004.

Char D. Available at: http://www.tumori.org/research.html. Accessed 12 March 2006.

Cirrone G, Cuttone G, Lojacono P, Lo Nigro S, Mongelli V, Patti I, Privitera G, Raffaele L, Rifuggiato D, Sabini M, Salamone V, Spatola C, Valastro L. A 62-MeV proton beam for the treatment of ocular melanoma at laboratori nazionali del Sud-INFN. IEEE Trans Nucl Sci 51(3):860-865; 2004.

Finger P. Available at: http://www.eyecancer.com/Content.aspx?sSection=Research &sSubSection=Content&sPage=Research.ascx&nID=23. Accessed 12 March 2006.

Godfrey DG, Waldron RG, Capone A Jr. Transpupillary thermotherapy for small choroidal melanoma. Am J Ophthalmol 128:88-93; 1999.

Harbour J. Clinical overview of uveal melanoma: introduction to tumors of the eye. New York: Marcel Dekker; 2003.

Heufelder J. How is the treatment done? Available at: http://www.hmi.de/isl/att/att-3_en.html. Accessed 10 March 2006.

Jones B, Errington R. Proton beam radiotherapy. Br J Radiol 73:802-805; 2000

Kimmel Cancer Center. Available at: http://www.kcc.tju.edu/Clinical/images/ UvealMelanoma.jpg. Accessed 12 March 2006.

Kooy H, Schaefer M, Rosenthal S, Bortfeld T. Monitor unit calculations for range-modulated spread-out Bragg peak fields. Phys Med Biol 48:2797-2808; 2003.

Levin WP, Kooy H, Loeffler JS, Delaney TF. Proton beam therapy. Br J Cancer 93(8):849-854; 2005.

Liu H. Application specific embedded system design for medical applications. Available at: http://www.nd.edu/~hliu/schoolpage/medical.html. Accessed 28 December 2005.

Macknight A, McLaughlin C, Peart D, Purves R, Carre D, Civan M. Formation of the aqueous humor. Clin Exp Pharmacol Physiol 27:100-107; 2000

Metropolis N, Ulam S. The Monte Carlo method. J Am Stat Assoc 44:335-341; 1949

Newhauser W, Koch N, Hummel S, Ziegler M, Titt U. Monte Carlo simulations of a nozzle for the treatment of ocular tumours with high-energy proton beams. Phys Med Biol 50:5229–5249; 2005.

Parsons JT, Bova FJ, Mendenhall WM, Million RR, Fitzgerald CR. Response of the normal eye to high dose radiotherapy. Oncology (Huntington) 10:837-847; 1996.

Pelowitz D (Ed.). MCNPXtm User's Manual Version 2.5.0, Los Alamos National Laboratory Report LA-CP-05-0369, 2005.

Robertson DM, Earle J, Anderson JA. Preliminary observations regarding the use of iodine-125 in the management of choroidal melanoma. Trans Ophthalmol Soc UK 103:155-160; 1983.

Shultis J, Faw R. An MCNP Primer. Available at: http://ww2.mne.ksu.edu/~jks/MCNPprmr.pdf. Accessed 3 January 2006.

Stys P, Lopachin R. Elemental composition and water content of rat optic nerve myelinated axons during in vitro post-anoxia reoxygenation. Neuroscience 73:1081-1090; 1996.

Wilson R. Radiological use of fast protons. Radiology 47:487–491; 1946.

Zaidi H. Therapeutic Applications of Monte Carlo Calculations in Nuclear Medicine. London: IOP Publishing Ltd; 2003.

Zimmerman LE, McLean IW, Foster WD. Does enucleation of the eye containing a malignant melanoma prevent or accelerate the dissemination of tumour cells. Br J Ophthalmol 62:420-425; 1978.

Supplemental Sources

Agosteo S, Birattari C, Caravaggio M, SilariMand G. Secondary neutron and photon dose in proton therapy. Radiother Oncol (48):293–305; 1998.

Bues M, Newhauser WD, Titt U, Smith AR. Proton beam shaping with a multi-leaf collimator: a Monte Carlo study. Radiat. Prot. Dosim. 2005 at press

Fontenot J, Newhauser WD, Titt U. Design tools for proton therapy nozzles based on the double-scattering foil technique. Radiat. Prot. Dosim. 116:211-215; 2005

Hendricks, McKinney JS, Waters GW, Roberts LS, Egdorf TL, Finch HW, Trellue JP, Pitcher HR, Mayo EJ, Swinhoe DR, Tobin MT, Durkee SJ, Gallmeier JW, David FX, Hamilton JC, Lebenhaft WB, J. MCNPX extensions version 2.5.0. Los Alamos National Laboratory Report LA-UR-04-0570; 2004.

Hughes G, Prael R, Little R. MCNPX—the LAHET/MCNP code merger technical report LA-UR-97-4891 Los Alamos National Laboratory, 1997

Jiang H, Paganetti H. Adaptation of GEANT4 to Monte Carlo dose calculations based on CT data. Med Phys 31:2811–2818; 2004

Medin J, Andreo P. Monte Carlo calculated stopping-power ratios, water/air, for clinical proton dosimetry (50–250 MeV). Phys Med Biol 42:89–105; 1997.

Munzenrider J, Verhey LJ, Gragoudas ES, Seddon JM, Urie M, Gentry R, Birnbaum S, Ruotolo DM, Crowell C, McManus P. Conservative treatment of uveal melanoma: local recurrence after proton beam therapy. Int J Radiat Oncol Biol Phys 17:493–8; 1989.

Newhauser WD, Titt U, Dexheimer D, Yan X, Nill S. Neutron shielding verification measurements and simulations for a 235-MeV proton therapy center. Nucl Instrum Methods A. 476:80–84; 1989.

Paganetti H. Calculation of the spatial variation of relative biological effectiveness in a therapeutic proton field for eye treatment. Phys Med Biol 43:2147–2157; 1998.

Paganetti H. Monte Carlo method to study the proton fluence for treatment planning. Med Phys 25:2370–2375; 1998.

Paganetti H, Jiang H, Adams JA, Chen GT, Rietzel E. Monte Carlo simulations with time-dependent geometries to investigate effects of organ motion with high temporal resolution. Int J Radiat Oncol Biol Phys 60:942–950; 2004.

Paganetti H, Jiang H, Lee SY, Kooy HM. Monte Carlo simulations for nozzle design, commissioning and quality assurance for a proton radiation therapy facility. Med Phys 31:2107–2118; 2004.

Palmans H, Symons JE, Denis JM, de Kock EA, Jones DT, Vynckier S. Fluence correction factors in plastic phantoms for clinical proton beams. Phys Med Biol 47:3055–3071; 2002.

Polf JC, Newhauser WD. Effect of range modulation on the neutron dose equivalent around a passive scattering proton therapy treatment nozzle. Phys Med Biol 50:3859–3873; 2005.

Prael R, Lichtenstein H. 1989 User's Guide to LCS: The LAHET code system technical report LA-UR-89-3014 Los Alamos, NM, Los Alamos National Laboratory; 1989.

Romero JL. Patient positioning for proton therapy using a proton range telescope. Nucl Instrum Methods A 356:558–565; 1995.

Sakae T, Nohtomi A, Maruhashi A, Sato M, Terunuma T, Kohno R, Akine Y, Hayakawa Y, Koike Y. Multi-layer energy filter for realizing conformal irradiation in charged particle therapy. Med Phys 27:368–373; 2000.

Schneider U, Agosteo S, Pedroni E, Besserer J. Secondary neutron dose during proton therapy using spot scanning. Int J Radiat Oncol Biol Phys 53:244–251; 2002.

Schulte RW, Bashkirov V, Loss-Klock MC, Li T, Wroe AJ, Evseev I, Williams DC, Satogata T. Density resolution of proton computed tomography. Med Phys 32:1035–1046; 2005.

Siebers J. Application of Monte Carlo to proton therapy radiation therapy. Proceedings from Advanced Monte Carlo for Radiation Physics, Particle Transport Simulations, and Applications. Lisbon: Nuclear Energy Agency; (New York: Springer) pp 1051–1056; 2000.

Simonova G, Novotny J, Liscak R, Pilbauer J. Leksell gamma knife treatment of uveal melanoma. J Neurosurg 97:635-639; 2002.

Suit HD. Protons to replace photons in external beam radiation therapy? Clin Oncol 15:S29-S31; 2002

Titt U, Newhauser WD. Neutron shielding in a proton therapy facility based on Monte Carlo simulations: the design method of choice. Radiat Prot Dosim at press; 2005.

Tourovsky A, Lomax AJ, Schneider U, Pedroni E. Monte Carlo dose calculations for spot scanned proton therapy. Phys Med Biol 50:971–981; 2005.

Urie M, Sisterson J, Koehler A, Goitein M, Zoesman J. Proton beam penumbra: effects of separation between patient and beam modifying devices. Med Phys 13:734–741; 1986.

Verhaegen F, Palmans H. A systematic Monte Carlo study of secondary electron fluence perturbation in clinical proton beams (70–250 MeV) for cylindrical and spherical ion chambers. Med Phys 28:2088–2095; 2001.

Wroe AJ, Cornelius IM, Rosenfeld AB. The role of nonelastic reactions in absorbed dose distributions from therapeutic proton beams in different medium. Med Phys 32:37–41; 2005.

Zaidi H. Therapeutic Applications of Monte Carlo Calculations in Nuclear Medicine. London: IOP Publishing Ltd; 2003.

APPENDIX A

Eye Model Dimensions

The model was constructed using concentric spheres with the dimensions listed in Fig. 14. The centers of the lens spheres were offset relative to the center of the outer eye wall by 0.446 cm and 0.246 cm. The spheres that constructed the cornea were both offset by 0.446 cm and varied in their radii, 1 cm and 0.75 cm, respectively. The optic nerve was simulated as a cylinder appropriately offset from the posterior pole of the eye by -0.247cm on the y-axis (to the left in Fig. 14) and 1.2195 cm on the z-axis (in the upward direction in Fig. 16).

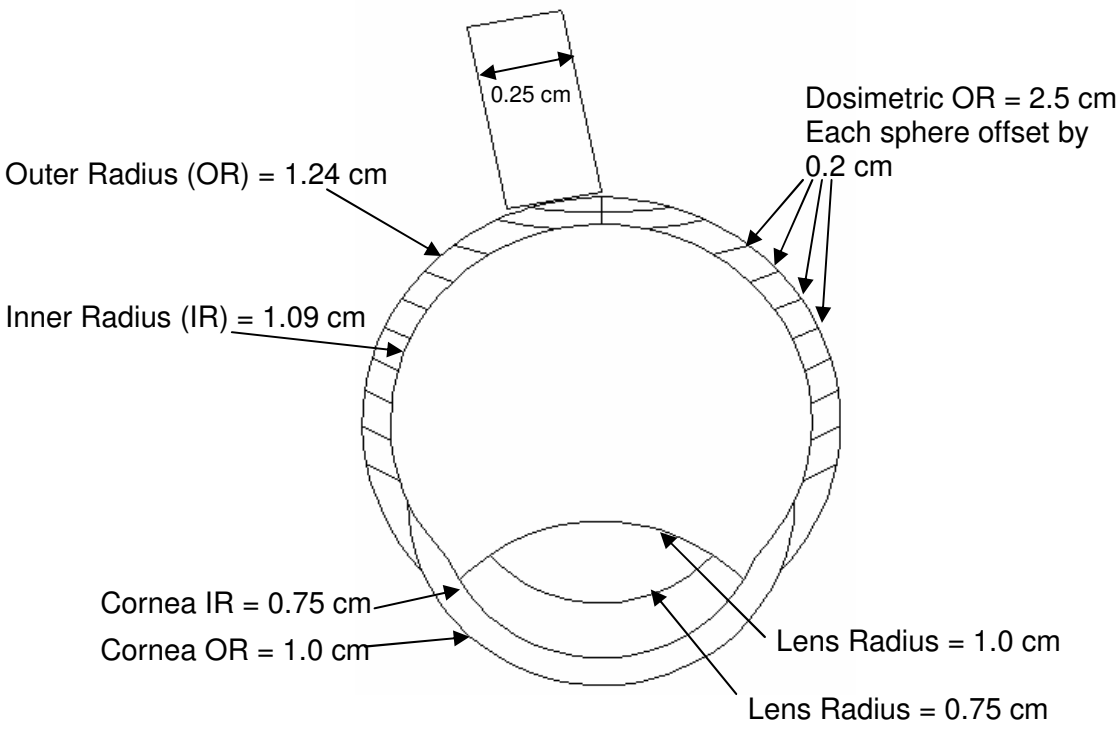

Fig 16: Dimensions of the eye model

APPENDIX B

Dosimetric Cells Volume Calculation

The MCNPX code has limited ability to compute the volumes of defined cells. The dosimetric volumes in the outer wall of the eye are an example of geometry too complex for MCNPX. Thus, the volumes had to be computed by hand, and input directly into the program. Equation 1 was used for calculating the volumes of overlapping spheres.

$$V = \frac{\pi(R + r - d)^2 (d^2 + 2dr - 3r^2 + 2dR + 6rR - 3R^2)}{12d} \tag{1}$$

where R and r are the radii of the larger and smaller spheres, respectively, and d is the distance between the centers. The overlapping volumes were calculated starting with the section closest to the optic nerve, then working successively forward. The previous volumes and the aqueous humor portion of the eye were subtracted from the volume of the new dosimetric cell. The results are shown in Table 4.

Table 4. Dosimetric Cell Volumes

Dosimetric Cells	Volume (cm^3)
29 and 39	0.0090
28 and 38	0.0322
27and 37	0.0760
26 and 36	0.0789
25 and 35	0.0822
24 and 34	0.0863
23 and 33	0.0914
22 and 32	0.0978
21 and 31	0.1059
20 and 30	0.1166

APPENDIX C

MCNPX Typical Case Output File

```
1mcnpx    version 2.5.0 ld=Mon Mar 21 08:00:00 MST 2005               03/24/06 01:02:32
 ******************************************************************************************  probid =   03/24/06 01:02:32
 i=shape

 ***************************************************
 *                                                 *
 *            Copyright Notice for MCNPX           *
 *                                                 *
 * This program was prepared by the Regents of the *
 * University of California at Los Alamos National *
 * Laboratory (the University) under contract number *
 * W-7405-ENG-36 with the U.S. Department of Energy *
 * (DOE).  The University has certain rights in the *
 * program pursuant to the contract and the program *
 * should not be copied or distributed outside your *
 * organization.   All rights in the program are    *
 * reserved by the DOE and the University.  Neither *
 * the U.S. Government nor the University makes any *
 * warranty, express or implied, or assumes any     *
 * liability or responsibility for the use of this  *
 * software.                                        *
 *                                                 *
 ***************************************************
    1-       Message: outp=eye.o runtpe=eye.r mctal=eye.m
    2-            datapath=/usr/local/mcnpx_2.5.0/mcnpxs
    3-
    4-       62-MeV SOBP Proton Beam with eye phantom.
    5-       1 3 -0.0012 -1 11 21 27 40:(-30 -31 11 27) imp:h 1 $ Outside the eye
    6-       2 0 1 imp:h 0 $ outside world
    7-       c
    8-       10 2 -1.07 (-21 20 11):(-21 20 -11 10) imp:h 1 $ corena
    9-       11 4 -1.03 -26 25 -20 imp:h 1 $ anterior chamber
   10-       12 2 -1.07 -25 -26 imp:h 1  $ lens
   11-       13 4 -1.03 (-10 25 26):(-10 -25 26):(26 -20 10):(-10 -21 20):(-10 -30 -31)
   12-                imp:h 1 $ vitreous
   13-       14 6 -1.04 -27 imp:h 1 $ Optic Nerve
   14-       c
   15-       15 5 -1.03 -11 10 21 20 30 31 imp:h 1 $ outer eye
   16-       c
   17-       20 5 -1.03 41 (-11 10 -30 31) vol=0.1166 imp:h 1 $ Anterior right
   18-       21 5 -1.03 41 (-11 10 -31 32) vol=0.1059 imp:h 1
   19-       22 5 -1.03 41 (-11 10 -32 33) vol=0.097805 imp:h 1
   20-       23 5 -1.03 41 (-11 10 -33 34) vol=0.09142 imp:h 1
   21-       24 5 -1.03 41 (-11 10 -34 35) vol=0.086345 imp:h 1
   22-       25 5 -1.03 41 (-11 10 -35 36) vol=0.08223 imp:h 1
   23-       26 5 -1.03 41 (-11 10 -36 37) vol=0.078855 imp:h 1
```

```
  24-       27 5 -1.03 41 (-11 10 -37 38) vol=0.076049 imp:h 1
  25-       28 5 -1.03 41 (-11 10 -38 39) vol=0.0321835 imp:h 1
  26-       29 5 -1.03 41 (-11 10 -39) vol=0.0089625 imp:h 1
  27-       30 5 -1.03 -41 (-11 10 -30 31) vol=0.1166 imp:h 1 $ Anterior left
  28-       31 5 -1.03 -41 (-11 10 -31 32) vol=0.1059 imp:h 1
  29-       32 5 -1.03 -41 (-11 10 -32 33) vol=0.097805 imp:h 1
  30-       33 5 -1.03 -41 (-11 10 -33 34) vol=0.09142 imp:h 1
  31-       34 5 -1.03 -41 (-11 10 -34 35) vol=0.086345 imp:h 1
  32-       35 5 -1.03 -41 (-11 10 -35 36) vol=0.08223 imp:h 1
  33-       36 5 -1.03 -41 (-11 10 -36 37) vol=0.078855 imp:h 1
  34-       37 5 -1.03 -41 (-11 10 -37 38) vol=0.076049 imp:h 1
  35-       38 5 -1.03 -41 (-11 10 -38 39) vol=0.0321835 imp:h 1
  36-       39 5 -1.03 -41 (-11 10 -39) vol=0.0089625 imp:h 1
  37-       40 1 -1 -40 imp:h 1
  38-
  39-       1 rcc 0 0 -10.1 0 0 30 20  $ Phantom boundry
  40-       10 sz 3.546 1.09 $ Choroid/Sclera innerwall
  41-       11 sz 3.546 1.2375 $ Choroid/Sclera outerwall
  42-       20 sz 3.1 .85 $inner cornea
  43-       21 sz 3.1 1.0 $outer cornea
  44-       25 sz 3.3 .75 $ outer lens
  45-       26 sz 2 1  $ inner lens
  46-       27 rcc -0.247 0 4.7655 -0.2 0 1 0.25  $ optic nerve
  47-       30 sz 5.5 2.5 $ Dosimetric spheres
  48-       31 sz 5.7 2.5
  49-       32 sz 5.9 2.5
  50-       33 sz 6.1 2.5
  51-       34 sz 6.3 2.5
  52-       35 sz 6.5 2.5
  53-       36 sz 6.7 2.5
  54-       37 sz 6.9 2.5
  55-       38 sz 7.1 2.5
  56-       39 sz 7.2 2.5
  57-       40 box -10 -10 0.5 20 0 0 0 20 0 0 0 -1.5
  58-       41 px 0
  59-
  60-       mode h n e
  61-       sdef pos 6 0 -2 erg d2 vec -1 0 1.12 axs -1 0 1.12 dir 1 ext 0 rad d1 par h
warning.  ext is constant.  in most problems it is a variable.
  62-       phys:h 70
  63-       si1 .5
  64-       si2 0 40.6502 40.7966 44.1944 47.5249 50.6795 53.6850 56.5626 59.3297 62
  65-       c
  66-       sp2 0 0.0509 .0020 0.0587 0.0665 0.0783 0.0902 0.1174 0.1448 0.3914
  67-       c
  68-       m1 1001 -0.11111 8016 -0.8889  $ Water
  69-       m2 1001 -9.6 6012 -19.5 7014 -5.7 8016 -64.6 11000 -0.1 15000 -0.1 16000 -0.3
  70-                17000 -0.1  $ Lens/Cornea (ro=1070kg/m3)
  71-       m3 7014  -9.06E-04   8016  -2.78E-04  $ air
  72-       m4 1001 -10.8 6012 -4.1 7014 -1.1 8016 -83.2 11000 -0.3 16000 -0.1
  73-               17000 -0.4 $ Anterior/Vitreous (ro=1030kg/m3)
  74-       m5 1001 -10.5 6012 -25.6 7014 -2.7 8016 -60.2 11000 -0.1 15000 -0.2 16000 -0.3
  75-               17000 -0.2 19000 -0.2 $Outer eye structure (ro=1030kg/m3)
  76-       m6 15000 -34.7 17000 -56.4 20000 -3.1 12000 -0.62 1001 -1.72
```

```
  77-               8016 -2.58 $ Nerve (ro=1040kg/m3)
  78-       F6:H 10 11 12 13 14 20 21 22 23 24 25 26 27 28 29 30 31 32
  79-            33 34 35 36 37 38 39
  80-       FC6 LOOK AT ME
  81-       nps 300000
  82-       prdmp 2j 1
  83-       c
  84-       c tmesh
  85-       c rmesh11:h flux
  86-       c cora11 -11 11
  87-       c corb11 -11 99i 11
  88-       c corc11 0 99i 30
  89-       c rmesh31:h pedep
  90-       c cora31 -11 11
  91-       c corb31 -11 99i 11
  92-       c corc31 0 99i 30
  93-       c endmd
  94-       c mplot freq 5000 plot ex 20 or 0 0 15
  95-       c      px 0 la 0 1 tal31 col on la 0 0 &
  96-       c      con 1e-4 .2 log
  97-

 warning.  neutron     importances have been set equal to 1.

 warning.  electron    importances have been set equal to 1.

 warning.  use models for the following missing data tables:
  11000.  c
  15000.  c
  11000.  h
  12000.  h
  15000.  h
  16000.  h
  17000.  h
  19000.  h
  20000.  h

 warning.    5 materials had unnormalized fractions. print table 40.


1LAHET physics options:                                                                                    print table 41

 lca    ielas   ipreq  iexisa  ichoic   jcoul  nexite   npidk   noact    icem
 lca        2       1       1      23       1       1       0       1       0

 lcb    flenb(i),i=1,6                                                          ctofe       flim0
 lcb    3.4900E+03  3.4900E+03  2.4900E+03  2.4900E+03  8.0000E+02  8.0000E+02 -1.0000E+00 -1.0000E+00

 lea     ipht     icc  nobalc  nobale   ifbrk  ilvden   ievap   nofis
 lea        1       4       1       0       1       0       0       1

 leb    yzere       bzere       yzero       bzero
 leb    1.5000E+00  8.0000E+00  1.5000E+00  1.0000E+01
```

```
 warning.  cross-section file bertin     does not exist.
1cells                                                                                                    print table 60
```

cell	mat	atom density	gram density	volume	mass	pieces	neutron importance	electron importance	proton importance
1	3	5.00973E-05	1.20000E-03	0.00000E+00	0.00000E+00	0	1.0000E+00	1.0000E+00	1.0000E+00
2	0	0.00000E+00	0.00000E+00	0.00000E+00	0.00000E+00	0	0.0000E+00	0.0000E+00	0.0000E+00
3	2	1.00623E-01	1.07000E+00	6.83139E-01	7.30959E-01	1	1.0000E+00	1.0000E+00	1.0000E+00
4	4	1.01510E-01	1.03000E+00	4.50999E-01	4.64529E-01	1	1.0000E+00	1.0000E+00	1.0000E+00
5	2	1.00623E-01	1.07000E+00	2.46823E-01	2.64100E-01	1	1.0000E+00	1.0000E+00	1.0000E+00
6	4	1.01510E-01	1.03000E+00	4.99775E+00	5.14768E+00	1	1.0000E+00	1.0000E+00	1.0000E+00
7	6	2.95831E-02	1.04000E+00	2.00238E-01	2.08248E-01	1	1.0000E+00	1.0000E+00	1.0000E+00
8	5	1.02588E-01	1.03000E+00	3.79608E-01	3.90996E-01	1	1.0000E+00	1.0000E+00	1.0000E+00
9	5	1.02588E-01	1.03000E+00	1.16600E-01	1.20098E-01	0	1.0000E+00	1.0000E+00	1.0000E+00
10	5	1.02588E-01	1.03000E+00	1.05900E-01	1.09077E-01	0	1.0000E+00	1.0000E+00	1.0000E+00
11	5	1.02588E-01	1.03000E+00	9.78050E-02	1.00739E-01	0	1.0000E+00	1.0000E+00	1.0000E+00
12	5	1.02588E-01	1.03000E+00	9.14200E-02	9.41626E-02	0	1.0000E+00	1.0000E+00	1.0000E+00
13	5	1.02588E-01	1.03000E+00	8.63450E-02	8.89354E-02	0	1.0000E+00	1.0000E+00	1.0000E+00
14	5	1.02588E-01	1.03000E+00	8.22300E-02	8.46969E-02	0	1.0000E+00	1.0000E+00	1.0000E+00
15	5	1.02588E-01	1.03000E+00	7.88550E-02	8.12206E-02	0	1.0000E+00	1.0000E+00	1.0000E+00
16	5	1.02588E-01	1.03000E+00	7.60490E-02	7.83305E-02	0	1.0000E+00	1.0000E+00	1.0000E+00
17	5	1.02588E-01	1.03000E+00	3.21835E-02	3.31490E-02	0	1.0000E+00	1.0000E+00	1.0000E+00
18	5	1.02588E-01	1.03000E+00	8.96250E-03	9.23137E-03	0	1.0000E+00	1.0000E+00	1.0000E+00
19	5	1.02588E-01	1.03000E+00	1.16600E-01	1.20098E-01	0	1.0000E+00	1.0000E+00	1.0000E+00
20	5	1.02588E-01	1.03000E+00	1.05900E-01	1.09077E-01	0	1.0000E+00	1.0000E+00	1.0000E+00
21	5	1.02588E-01	1.03000E+00	9.78050E-02	1.00739E-01	0	1.0000E+00	1.0000E+00	1.0000E+00
22	5	1.02588E-01	1.03000E+00	9.14200E-02	9.41626E-02	0	1.0000E+00	1.0000E+00	1.0000E+00
23	5	1.02588E-01	1.03000E+00	8.63450E-02	8.89354E-02	0	1.0000E+00	1.0000E+00	1.0000E+00
24	5	1.02588E-01	1.03000E+00	8.22300E-02	8.46969E-02	0	1.0000E+00	1.0000E+00	1.0000E+00
25	5	1.02588E-01	1.03000E+00	7.88550E-02	8.12206E-02	0	1.0000E+00	1.0000E+00	1.0000E+00
26	5	1.02588E-01	1.03000E+00	7.60490E-02	7.83305E-02	0	1.0000E+00	1.0000E+00	1.0000E+00
27	5	1.02588E-01	1.03000E+00	3.21835E-02	3.31490E-02	0	1.0000E+00	1.0000E+00	1.0000E+00
28	5	1.02588E-01	1.03000E+00	8.96250E-03	9.23137E-03	0	1.0000E+00	1.0000E+00	1.0000E+00
29	1	9.98573E-02	1.00000E+00	6.00000E+02	6.00000E+02	0	1.0000E+00	1.0000E+00	1.0000E+00
total				6.08511E+02	6.08806E+02				

```
 random number control    0.830205014835200E+14

    minimum source weight = 9.9875E-01    maximum source weight = 1.0000E+00

        6 warning messages so far.
1cross-section tables                                                                                     print table 100

     table    length

                       tables from file actia

 particle-production data for ipt= 31 being expunged from   1001.62c
 no particle-production data for ipt=  9 from   1001.62c
   1001.62c    5202  1-h-1 at 293.6K from endf-vi.8 njoy99.50                                  mat 125      12/05/01
```

```
particle-production data for ipt=  9 being used from   7014.62c
particle-production data for ipt= 31 being expunged from   7014.62c
particle-production data for ipt= 34 being expunged from   7014.62c
  7014.62c   73728  7-n-14 at 293.6K from endf-vi.8 njoy99.50                    mat 725      12/05/01
particle-production data for ipt=  9 being used from   8016.62c
particle-production data for ipt= 31 being expunged from   8016.62c
particle-production data for ipt= 32 being expunged from   8016.62c
particle-production data for ipt= 34 being expunged from   8016.62c
  8016.62c  186551  8-o-16 at 293.6K from endf-vi.8 njoy99.50                    mat 825      12/05/01
no particle-production data for ipt=  9 from  12000.62c
 12000.62c   44838  12-mg-0 at 293.6K from endf/b-vi.8 njoy99.50                 mat1200      12/06/01
no particle-production data for ipt=  9 from  16000.62c
 16000.62c   68665  16-s-0 at 293.6K from endf/b-vi.8 njoy99.50                  mat1600      12/06/01
no particle-production data for ipt=  9 from  19000.62c
 19000.62c   26425  19-k-0 at 293.6K from endf/b-vi.8 njoy99.50                  mat1900      12/06/01
particle-production data for ipt=  9 being used from  20000.62c
particle-production data for ipt= 31 being expunged from  20000.62c
particle-production data for ipt= 32 being expunged from  20000.62c
particle-production data for ipt= 34 being expunged from  20000.62c
 20000.62c   77701  20-ca-0 at 293.6K from endf-vi.8 njoy99.50                   mat2000      12/05/01

                     tables from file rmccs

no particle-production data for ipt=  9 from   6012.50c
  6012.50c   16126  njoy                                                  (  1306)      79/07/31.

                     tables from file endf66a

no particle-production data for ipt=  9 from  17000.66c
 17000.66c   25119  17-cl-0 at 293.6K from endf-vi.0 njoy99.50                  mat1700      07/25/01

                     tables from file la150h

  1001.24h   15895  1-h-1 apt la150 njoy 99.20 mcnpx                           mat 125      09/27/00
  6012.24h   51762  6-c-12 apt la150 njoy 99.20 mcnpx                          mat 625      09/27/00
  7014.24h   71369  7-n-14 apt la150 njoy 99.20 mcnpx                          mat 725      09/27/00
  8016.24h   54535  8-o-16 apt la150 njoy 99.20 mcnpx                          mat 825      09/27/00

 total      717916

maximum photon energy set to   70.0 mev (maximum electron energy)

                     tables from file el03

  1000.03e    2329                                                                        6/6/98
  6000.03e    2333                                                                        6/6/98
  7000.03e    2333                                                                        6/6/98
  8000.03e    2333                                                                        6/6/98
 11000.03e    2337                                                                        6/6/98
 12000.03e    2337                                                                        6/6/98
 15000.03e    2339                                                                        6/6/98
 16000.03e    2339                                                                        6/6/98
 17000.03e    2339                                                                        6/6/98
 19000.03e    2343                                                                        6/6/98
```

1particles and energy limits print table 101

particle type	particle cutoff energy	maximum particle energy	smallest table maximum	largest table maximum	always use table below	always use model above
1 n neutron	0.0000E+00	1.0000E+37	2.0000E+01	1.5000E+02	0.0000E+00	1.5000E+02
3 e electron	1.0000E-03	7.0000E+01	7.0000E+01	7.0000E+01	1.0000E+37	1.0000E+37
9 h proton	1.0000E+00	7.0000E+01	1.5000E+02	1.5000E+02	0.0000E+00	1.5000E+02

The following nuclides use physics models rather than data tables:

11000. c
15000. c
11000. h
12000. h
15000. h
16000. h
17000. h
19000. h
20000. h

decimal words of dynamically allocated storage

general	0	
tallies	3404	
bank	71041	
cross sections	717917	
total	0	= 0 bytes

dump no. 1 on file eye.r nps = 0 coll = 0 ctm = 0.00 nrn = 0

6 warning messages so far.

1problem summary

run terminated when 300000 particle histories were done.

+ 03/24/06 01:23:38

62-MeV SOBP Proton Beam with eye phantom. probid = 03/24/06 01:02:32

neutron creation	tracks	weight (per source particle)	energy	neutron loss	tracks	weight (per source particle)	energy
source	0	0.	0.	escape	2096	6.9239E-03	5.5676E-02

nucl. interaction	0	0.	0.
particle decay	0	0.	0.
weight window	0	0.	0.
cell importance	0	0.	0.
weight cutoff	0	0.	0.
energy importance	0	0.	0.
dxtran	0	0.	0.
forced collisions	0	0.	0.
exp. transform	0	0.	0.
upscattering	0	0.	1.1226E-12
photonuclear	0	0.	0.
(n,xn)	0	0.	0.
prompt fission	0	0.	0.
delayed fission	0	0.	0.
tabular boundary	0	0.	0.
tabular sampling	2096	6.9779E-03	6.1935E-02
total	2096	6.9779E-03	6.1935E-02

energy cutoff	0	0.	0.
time cutoff	0	0.	0.
weight window	0	0.	0.
cell importance	0	0.	0.
weight cutoff	0	0.	0.
energy importance	0	0.	0.
dxtran	0	0.	0.
forced collisions	0	0.	0.
exp. transform	0	0.	0.
downscattering	0	0.	5.6441E-03
capture	0	5.4061E-05	6.1521E-04
loss to (n,xn)	0	0.	0.
loss to fission	0	0.	0.
nucl. interaction	0	0.	0.
particle decay	0	0.	0.
tabular boundary	0	0.	0.
total	2096	6.9779E-03	6.1935E-02

number of neutrons banked	2096
neutron tracks per source particle	6.9867E-03
neutron collisions per source particle	3.8133E-03
total neutron collisions	1144
net multiplication	0.0000E+00 0.0000

average time of (shakes)	
escape	1.6082E+01
capture	1.5248E+01
capture or escape	1.6076E+01
any termination	1.6076E+01

cutoffs	
tco	1.0000E+34
eco	0.0000E+00
wc1	-5.0000E-01
wc2	-2.5000E-01

electron creation	tracks	weight (per source particle)	energy (per source particle)
source	0	0.	0.
nucl. interaction	0	0.	0.
particle decay	0	0.	0.
weight window	0	0.	0.
cell importance	0	0.	0.
weight cutoff	0	0.	0.
energy importance	0	0.	0.
pair production	0	0.	0.
compton recoil	0	0.	0.
photo-electric	0	0.	0.
photon auger	0	0.	0.
electron auger	0	0.	0.
knock-on	0	0.	0.
(gamma,xelectron)	0	0.	0.
total	0	0.0000E+00	0.0000E+00

electron loss	tracks	weight (per source particle)	energy (per source particle)
escape	0	0.	0.
energy cutoff	0	0.	0.
time cutoff	0	0.	0.
weight window	0	0.	0.
cell importance	0	0.	0.
weight cutoff	0	0.	0.
energy importance	0	0.	0.
scattering	0	0.	0.
bremsstrahlung	0	0.	0.
interact or decay	0	0.	0.
total	0	0.0000E+00	0.0000E+00

number of electrons banked	0
electron tracks per source particle	0.0000E+00
electron substeps per source particle	0.0000E+00
total electron substeps	0

cutoffs	
tco	1.0000E+34
eco	1.0000E-03
wc1	0.0000E+00
wc2	0.0000E+00

proton creation	tracks	weight (per source particle)	energy (per source particle)
source	300000	9.9875E-01	5.3862E+01

proton loss	tracks	weight (per source particle)	energy (per source particle)
escape	52666	1.7533E-01	4.1278E+00

nucl. interaction	0	0.	0.
particle decay	0	0.	0.
weight window	0	0.	0.
cell importance	0	0.	0.
weight cutoff	0	0.	0.
energy importance	0	0.	0.
dxtran	0	0.	0.
forced collisions	0	0.	0.
exp. transform	0	0.	0.
tabular sampling	11971	3.9853E-02	4.8904E-01
photonuclear	0	0.	0.
elastic recoil	0	0.	0.
(gamma,xgen_chg)	0	0.	0.
total	311971	1.0386E+00	5.4351E+01

energy cutoff	248399	8.2696E-01	8.2621E-01
time cutoff	0	0.	0.
weight window	0	0.	0.
cell importance	0	0.	0.
weight cutoff	0	0.	0.
energy importance	0	0.	0.
dxtran	0	0.	0.
forced collisions	0	0.	0.
exp. transform	0	0.	0.
multiple scatter	0	0.	4.7604E+01
bremsstrahlung	0	0.	0.
nucl. interaction	0	0.	0.
elastic scatter	0	0.	4.5903E-01
particle decay	0	0.	0.
capture	62	2.0641E-04	3.5225E-03
tabular sampling	10844	3.6101E-02	1.3303E+00
total	311971	1.0386E+00	5.4351E+01

number of particles banked	11971
particle tracks per source particle	1.0399E+00
particle substeps per source particle	1.1777E+02
total particle substeps	35332483

cutoffs

tco	1.0000E+34
eco	1.0000E+00
wc1	0.0000E+00
wc2	0.0000E+00

computer time so far in this run	10.78 minutes
computer time in mcrun	10.71 minutes
source particles per minute	2.8009E+04
random numbers generated	197596640

maximum number ever in bank	3
bank overflows to backup file	0
dynamic storage	0 words, 0 bytes.
most random numbers used was	1482 in history 108072

range of sampled source weights = 9.9875E-01 to 9.9875E-01

lneutron activity in each cell print table 126

	cell	tracks entering	population	collisions	collisions * weight (per history)	number weighted energy	flux weighted energy	average track weight (relative)	average track mfp (cm)
1	1	2197	2096	3	9.5577E-06	2.6639E-01	8.5066E+00	9.9159E-01	1.2479E+04
3	10	71	69	4	1.3181E-05	6.6200E-01	7.1385E+00	9.9663E-01	6.3204E+00
4	11	26	25	1	3.3290E-06	1.8818E+00	9.0138E+00	9.9873E-01	7.1164E+00
5	12	17	17	2	6.6532E-06	1.6060E+00	7.9942E+00	9.9865E-01	6.6719E+00
6	13	96	145	48	1.5668E-04	1.2492E-02	6.6101E+00	9.9200E-01	6.0569E+00
7	14	6	6	0	0.0000E+00	6.9884E+00	1.0198E+01	9.9875E-01	1.7283E+01
8	15	54	65	2	6.6582E-06	2.6118E-01	5.4986E+00	9.9660E-01	5.4422E+00
9	20	37	52	3	9.9875E-06	1.0478E-01	5.9832E+00	9.9863E-01	6.0094E+00
10	21	38	49	0	0.0000E+00	1.6721E-01	6.8494E+00	9.9869E-01	6.5181E+00
11	22	31	41	3	9.6168E-06	1.2010E-02	6.3468E+00	9.9639E-01	6.2129E+00
12	23	23	27	0	0.0000E+00	7.3667E-02	8.3416E+00	9.9709E-01	6.8031E+00
13	24	23	25	1	3.3291E-06	1.8268E-02	7.2851E+00	9.9332E-01	5.4640E+00
14	25	25	30	2	6.6582E-06	1.4518E+00	7.0456E+00	9.9874E-01	6.1203E+00
15	26	22	24	0	0.0000E+00	1.2291E+00	6.2543E+00	9.9874E-01	5.6808E+00
16	27	19	19	2	6.5782E-06	1.1216E-02	8.4809E+00	9.9766E-01	6.8697E+00
17	28	10	10	0	0.0000E+00	5.1351E+00	7.5593E+00	9.9875E-01	6.4020E+00
18	29	5	5	0	0.0000E+00	5.6927E+00	9.7787E+00	9.9875E-01	6.9569E+00
19	30	9	9	0	0.0000E+00	2.5915E-02	1.2581E+01	9.9816E-01	7.8360E+00

20	31	7	7	0	0.0000E+00	4.8993E-03	7.0544E+00	9.9680E-01	4.9151E+00
21	32	6	6	0	0.0000E+00	1.8636E+01	2.0388E+01	9.9875E-01	1.1005E+01
22	33	10	10	0	0.0000E+00	1.7628E+00	1.0839E+01	9.9874E-01	8.1253E+00
23	34	10	10	0	0.0000E+00	7.1989E-01	8.7047E+00	9.9678E-01	6.7408E+00
24	35	13	13	1	3.3292E-06	4.0138E+00	7.6367E+00	9.7530E-01	6.7922E+00
25	36	4	4	2	6.6481E-06	2.7047E+00	3.0605E+00	9.9771E-01	4.8236E+00
26	37	5	5	3	9.8976E-06	8.2554E-04	4.0362E+00	9.9281E-01	4.6253E+00
27	38	5	5	0	0.0000E+00	5.9032E+00	6.1437E+00	9.9875E-01	6.6731E+00
28	39	5	5	0	0.0000E+00	5.0137E+00	7.4847E+00	9.9875E-01	6.1975E+00
29	40	45	1993	1067	3.5388E-03	3.8800E-01	8.6357E+00	9.9236E-01	7.2543E+00
total		2819	4772	1144	3.7909E-03				

1electron activity in each cell print table 126

	cell	tracks entering	population	substeps	substeps * weight (per history)	number weighted energy	flux weighted energy	average track weight (relative)	average track mfp (cm)
1	1	0	0	0	0.0000E+00	0.0000E+00	0.0000E+00	0.0000E+00	0.0000E+00
3	10	0	0	0	0.0000E+00	0.0000E+00	0.0000E+00	0.0000E+00	0.0000E+00
4	11	0	0	0	0.0000E+00	0.0000E+00	0.0000E+00	0.0000E+00	0.0000E+00
5	12	0	0	0	0.0000E+00	0.0000E+00	0.0000E+00	0.0000E+00	0.0000E+00
6	13	0	0	0	0.0000E+00	0.0000E+00	0.0000E+00	0.0000E+00	0.0000E+00
7	14	0	0	0	0.0000E+00	0.0000E+00	0.0000E+00	0.0000E+00	0.0000E+00
8	15	0	0	0	0.0000E+00	0.0000E+00	0.0000E+00	0.0000E+00	0.0000E+00
9	20	0	0	0	0.0000E+00	0.0000E+00	0.0000E+00	0.0000E+00	0.0000E+00
10	21	0	0	0	0.0000E+00	0.0000E+00	0.0000E+00	0.0000E+00	0.0000E+00
11	22	0	0	0	0.0000E+00	0.0000E+00	0.0000E+00	0.0000E+00	0.0000E+00
12	23	0	0	0	0.0000E+00	0.0000E+00	0.0000E+00	0.0000E+00	0.0000E+00
13	24	0	0	0	0.0000E+00	0.0000E+00	0.0000E+00	0.0000E+00	0.0000E+00
14	25	0	0	0	0.0000E+00	0.0000E+00	0.0000E+00	0.0000E+00	0.0000E+00
15	26	0	0	0	0.0000E+00	0.0000E+00	0.0000E+00	0.0000E+00	0.0000E+00
16	27	0	0	0	0.0000E+00	0.0000E+00	0.0000E+00	0.0000E+00	0.0000E+00
17	28	0	0	0	0.0000E+00	0.0000E+00	0.0000E+00	0.0000E+00	0.0000E+00
18	29	0	0	0	0.0000E+00	0.0000E+00	0.0000E+00	0.0000E+00	0.0000E+00
19	30	0	0	0	0.0000E+00	0.0000E+00	0.0000E+00	0.0000E+00	0.0000E+00
20	31	0	0	0	0.0000E+00	0.0000E+00	0.0000E+00	0.0000E+00	0.0000E+00
21	32	0	0	0	0.0000E+00	0.0000E+00	0.0000E+00	0.0000E+00	0.0000E+00
22	33	0	0	0	0.0000E+00	0.0000E+00	0.0000E+00	0.0000E+00	0.0000E+00
23	34	0	0	0	0.0000E+00	0.0000E+00	0.0000E+00	0.0000E+00	0.0000E+00
24	35	0	0	0	0.0000E+00	0.0000E+00	0.0000E+00	0.0000E+00	0.0000E+00
25	36	0	0	0	0.0000E+00	0.0000E+00	0.0000E+00	0.0000E+00	0.0000E+00
26	37	0	0	0	0.0000E+00	0.0000E+00	0.0000E+00	0.0000E+00	0.0000E+00
27	38	0	0	0	0.0000E+00	0.0000E+00	0.0000E+00	0.0000E+00	0.0000E+00
28	39	0	0	0	0.0000E+00	0.0000E+00	0.0000E+00	0.0000E+00	0.0000E+00
29	40	0	0	0	0.0000E+00	0.0000E+00	0.0000E+00	0.0000E+00	0.0000E+00
total		0	0	0	0.0000E+00				

1proton activity in each cell print table 126

cell	tracks entering	population	substeps	substeps * weight (per history)	number weighted energy	flux weighted energy	average track weight (relative)	average track mfp (cm)
1	557559	301058	695117	2.3142E+00	2.6328E+01	3.0541E+01	9.9875E-01	5.2397E+01
10	31119	31147	215984	7.1905E-01	2.2952E+01	2.5309E+01	9.9875E-01	3.4902E-02
11	671	673	27157	9.0410E-02	1.6165E+01	1.8331E+01	9.9875E-01	2.0743E-02
12	353	353	18350	6.1090E-02	1.2620E+01	1.4422E+01	9.9875E-01	1.3239E-02
13	156553	158123	16036181	5.3387E+01	1.6438E+01	1.8726E+01	9.9875E-01	2.1674E-02
14	6122	6123	300642	1.0009E+00	1.3675E+01	1.6629E+01	9.9875E-01	1.4599E-02
15	95361	95520	629683	2.0963E+00	2.5894E+01	2.7812E+01	9.9875E-01	4.1639E-02
20	84117	84237	506589	1.6865E+00	2.5765E+01	2.7606E+01	9.9875E-01	4.1012E-02
21	69258	69393	452732	1.5072E+00	2.5645E+01	2.7457E+01	9.9875E-01	4.0583E-02
22	53213	53322	399228	1.3291E+00	2.5168E+01	2.6997E+01	9.9875E-01	3.9436E-02
23	39975	40032	365518	1.2169E+00	2.4286E+01	2.6145E+01	9.9875E-01	3.7338E-02
24	30271	30279	369738	1.2309E+00	2.2747E+01	2.4668E+01	9.9875E-01	3.3827E-02
25	25635	25494	429902	1.4312E+00	2.0149E+01	2.2045E+01	9.9875E-01	2.7885E-02
26	26072	26130	629841	2.0968E+00	1.5556E+01	1.7373E+01	9.9875E-01	1.8564E-02
27	17779	17797	737338	2.4547E+00	1.0089E+01	1.1675E+01	9.9875E-01	9.4447E-03
28	2329	2330	67055	2.2324E-01	6.0060E+00	6.9734E+00	9.9875E-01	3.7959E-03
29	13	13	302	1.0054E-03	5.5308E+00	6.6951E+00	9.9875E-01	3.7146E-03
30	32	32	1549	5.1569E-03	1.1036E+01	1.2697E+01	9.9875E-01	1.0908E-02
31	29	29	892	2.9696E-03	1.0823E+01	1.2424E+01	9.9875E-01	1.0335E-02
32	16	17	836	2.7832E-03	7.4239E+00	8.5565E+00	9.9875E-01	5.3970E-03
33	5	5	270	8.9887E-04	4.5967E+00	5.1886E+00	9.9875E-01	2.1469E-03
34	2	2	111	3.6954E-04	3.3992E+00	3.6795E+00	9.9875E-01	1.1208E-03
35	0	0	0	0.0000E+00	0.0000E+00	0.0000E+00	0.0000E+00	0.0000E+00
36	0	0	0	0.0000E+00	0.0000E+00	0.0000E+00	0.0000E+00	0.0000E+00
37	0	0	0	0.0000E+00	0.0000E+00	0.0000E+00	0.0000E+00	0.0000E+00
38	0	0	0	0.0000E+00	0.0000E+00	0.0000E+00	0.0000E+00	0.0000E+00
39	0	0	0	0.0000E+00	0.0000E+00	0.0000E+00	0.0000E+00	0.0000E+00
40	299908	309260	13447468	4.4769E+01	4.0192E+01	4.2637E+01	9.9875E-01	9.2409E-02
total	1496392	1251369	35332483	1.1763E+02				

1tally 6 nps = 300000

\+ LOOK AT ME

tally type 6 energy deposition units mev/gram

particle(s): proton

masses

cell:	10	11	12	13	14	20	21
	7.30959E-01	4.64529E-01	2.64100E-01	5.14768E+00	2.08248E-01	1.20098E-01	1.09077E-01
cell:	22	23	24	25	26	27	28
	1.00739E-01	9.41626E-02	8.89354E-02	8.46969E-02	8.12206E-02	7.83305E-02	3.31490E-02
cell:	29	30	31	32	33	34	35
	9.23137E-03	1.20098E-01	1.09077E-01	1.00739E-01	9.41626E-02	8.89354E-02	8.46969E-02
cell:	36	37	38	39			
	8.12206E-02	7.83305E-02	3.31490E-02	9.23137E-03			

cell 10

3.00521E-01 0.0080

```
cell  11
                4.56155E-02 0.0442
cell  12
                4.53162E-02 0.0625
cell  13
                2.46290E+00 0.0019
cell  14
                5.31604E-01 0.0165
cell  20
                5.49393E+00 0.0040
cell  21
                5.42271E+00 0.0044
cell  22
                5.11529E+00 0.0050
cell  23
                4.84849E+00 0.0057
cell  24
                4.82968E+00 0.0064
cell  25
                5.24439E+00 0.0067
cell  26
                6.24120E+00 0.0067
cell  27
                5.10333E+00 0.0084
cell  28
                7.76997E-01 0.0254
cell  29
                1.13106E-02 0.3538
cell  30
                7.58366E-03 0.2011
cell  31
                4.60522E-03 0.2329
cell  32
                3.71142E-03 0.2952
cell  33
                1.00003E-03 0.4976
```

```
 cell  34
                3.87863E-04 0.7141

 cell  35
                0.00000E+00 0.0000

 cell  36
                0.00000E+00 0.0000

 cell  37
                0.00000E+00 0.0000

 cell  38
                0.00000E+00 0.0000

 cell  39
                0.00000E+00 0.0000
1analysis of the results in the tally fluctuation chart bin (tfc) for tally   6 with nps =    300000    print table 160


 normed average tally per history  = 3.00521E-01          unnormed average tally per history  = 2.19669E-01
 estimated tally relative error    = 0.0080               estimated variance of the variance  = 0.0004
 relative error from zero tallies  = 0.0054               relative error from nonzero scores  = 0.0059

 number of nonzero history tallies =       31100          efficiency for the nonzero tallies  = 0.1037
 history number of largest  tally  =       47958          largest  unnormalized history tally = 3.17555E+01
 (largest  tally)/(average tally)  = 1.44561E+02          (largest  tally)/(avg nonzero tally)= 1.49861E+01

 (confidence interval shift)/mean  = 0.0001               shifted confidence interval center  = 3.00540E-01


 if the largest  history score sampled so far were to occur on the next history, the tfc bin quantities would change as follows:

      estimated quantities           value at nps           value at nps+1           value(nps+1)/value(nps)-1.

      mean                            3.00521E-01            3.00665E-01                    0.000479
      relative error                  7.96772E-03            7.97823E-03                    0.001319
      variance of the variance        4.24576E-04            4.34411E-04                    0.023164
      shifted center                  3.00540E-01            3.00540E-01                    0.000001
      figure of merit                 1.47065E+03            1.46677E+03                   -0.002634

 the estimated inverse power slope of the 200 largest  tallies starting at 1.13630E+01 is 3.4002
 the large score tail of the empirical history score probability density function appears to have no unsampled regions.
```

==========

          results of 10 statistical checks for the estimated answer for the tally fluctuation chart (tfc) bin of tally   6

tfc bin	--mean--	---------relative error---------			----variance of the variance----			--figure of merit--		-pdf-
behavior	behavior	value	decrease	decrease rate	value	decrease	decrease rate	value	behavior	slope
desired	random	<0.10	yes	1/sqrt(nps)	<0.10	yes	1/nps	constant	random	>3.00
observed	random	0.01	yes	yes	0.00	yes	yes	constant	random	3.40
passed?	yes	yes	yes	yes	yes	yes	yes	yes	yes	yes

==========

 this tally meets the statistical criteria used to form confidence intervals: check the tally fluctuation chart to verify.
 the results in other bins associated with this tally may not meet these statistical criteria.

 estimated asymmetric confidence interval(1,2,3 sigma): 2.9815E-01 to 3.0293E-01; 2.9575E-01 to 3.0533E-01; 2.9336E-01 to 3.0772E-01
 estimated symmetric confidence interval(1,2,3 sigma): 2.9813E-01 to 3.0292E-01; 2.9573E-01 to 3.0531E-01; 2.9334E-01 to 3.0770E-01

 fom = (histories/minute)*(f(x) signal-to-noise ratio)**2 = (2.801E+04)*(2.291E-01)**2 = (2.801E+04)*(5.251E-02) = 1.471E+03
1status of the statistical checks used to form confidence intervals for the mean for each tally bin

 tally   result of statistical checks for the tfc bin (the first check not passed is listed) and error magnitude check for all bins

     6   passed the 10 statistical checks for the tally fluctuation chart bin result
         missed all bin error check: 25 tally bins had   5 bins with zeros and   6 bins with relative errors exceeding 0.10

 the 10 statistical checks are only for the tally fluctuation chart bin and do not apply to other tally bins.

 the tally bins with zeros may or may not be correct: compare the source, cutoffs, multipliers, et cetera with the tally bins.

 warning.   1 of the   1 tallies had bins with relative errors greater than recommended.
1tally fluctuation charts

	tally 6				
nps	mean	error	vov	slope	fom
16000	3.0470E-01	0.0358	0.0108	5.4	1365
32000	2.9756E-01	0.0250	0.0043	7.5	1396
48000	2.9725E-01	0.0205	0.0033	4.1	1385
64000	3.0126E-01	0.0176	0.0023	3.8	1404
80000	3.0054E-01	0.0158	0.0018	3.9	1407
96000	2.9889E-01	0.0143	0.0014	3.4	1422
112000	2.9739E-01	0.0132	0.0012	3.3	1439
128000	2.9822E-01	0.0123	0.0011	3.5	1438
144000	2.9816E-01	0.0116	0.0009	3.2	1454
160000	2.9913E-01	0.0110	0.0008	2.8	1460
176000	2.9833E-01	0.0105	0.0007	2.6	1456
192000	2.9867E-01	0.0100	0.0007	2.7	1456
208000	2.9932E-01	0.0096	0.0006	2.6	1466

```
   224000   2.9946E-01 0.0092 0.0005  2.8    1467
   240000   2.9932E-01 0.0089 0.0005  2.7    1468
   256000   2.9942E-01 0.0087 0.0005  2.9    1459
   272000   2.9950E-01 0.0084 0.0005  3.1    1466
   288000   3.0028E-01 0.0081 0.0004  3.0    1468
   300000   3.0052E-01 0.0080 0.0004  3.4    1471

************************************************************************************************************************
dump no.    2 on file eye.r        nps =      300000   coll =       35333627     ctm =   10.71     nrn =      197596640

tally data written to file eye.m

        7 warning messages so far.


run terminated when    300000 particle histories were done.

computer time =   10.78 minutes

mcnpx    version 2.5.0 Mon Mar 21 08:00:00 MST 2005               03/24/06 01:23:38     probid =   03/24/06 01:02:32
```

MCNPX Worst Case Output File

```
1mcnpx    version 2.5.0 ld=Mon Mar 21 08:00:00 MST 2005               03/24/06 00:34:52
 ******************************************************************************************  probid =   03/24/06 00:34:52
 i=shape

 ***************************************************
 *                                                 *
 *            Copyright Notice for MCNPX           *
 *                                                 *
 * This program was prepared by the Regents of the *
 * University of California at Los Alamos National *
 * Laboratory (the University) under contract number *
 * W-7405-ENG-36 with the U.S. Department of Energy *
 * (DOE).  The University has certain rights in the *
 * program pursuant to the contract and the program *
 * should not be copied or distributed outside your *
 * organization.   All rights in the program are    *
 * reserved by the DOE and the University.  Neither *
 * the U.S. Government nor the University makes any *
 * warranty, express or implied, or assumes any     *
 * liability or responsibility for the use of this  *
 * software.                                        *
 *                                                 *
 ***************************************************
    1-       Message: outp=eye.o runtpe=eye.r mctal=eye.m
    2-            datapath=/usr/local/mcnpx_2.5.0/mcnpxs
    3-
    4-       62-MeV SOBP Proton Beam with eye phantom.
    5-       1 3 -0.0012 -1 11 21 27 40:(-30 -31 11 27) imp:h 1 $ Outside the eye
    6-       2 0 1 imp:h 0 $ outside world
    7-       c
    8-       10 2 -1.07 (-21 20 11):(-21 20 -11 10) imp:h 1 $ corena
    9-       11 4 -1.03 -26 25 -20 imp:h 1 $ anterior chamber
   10-       12 2 -1.07 -25 -26 imp:h 1  $ lens
   11-       13 4 -1.03 (-10 25 26):(-10 -25 26):(26 -20 10):(-10 -21 20):(-10 -30 -31)
   12-                  imp:h 1 $ vitreous
   13-       14 6 -1.04 -27 imp:h 1 $ Optic Nerve
   14-       c
   15-       15 5 -1.03 -11 10 21 20 30 31 imp:h 1 $ outer eye
   16-       c
   17-       20 5 -1.03 41 (-11 10 -30 31) vol=0.1166 imp:h 1 $ Anterior right
   18-       21 5 -1.03 41 (-11 10 -31 32) vol=0.1059 imp:h 1
   19-       22 5 -1.03 41 (-11 10 -32 33) vol=0.097805 imp:h 1
   20-       23 5 -1.03 41 (-11 10 -33 34) vol=0.09142 imp:h 1
   21-       24 5 -1.03 41 (-11 10 -34 35) vol=0.086345 imp:h 1
   22-       25 5 -1.03 41 (-11 10 -35 36) vol=0.08223 imp:h 1
   23-       26 5 -1.03 41 (-11 10 -36 37) vol=0.078855 imp:h 1
   24-       27 5 -1.03 41 (-11 10 -37 38) vol=0.076049 imp:h 1
   25-       28 5 -1.03 41 (-11 10 -38 39) vol=0.0321835 imp:h 1
   26-       29 5 -1.03 41 (-11 10 -39) vol=0.0089625 imp:h 1
   27-       30 5 -1.03 -41 (-11 10 -30 31) vol=0.1166 imp:h 1 $ Anterior left
```

```
  28-       31 5 -1.03 -41 (-11 10 -31 32) vol=0.1059 imp:h 1
  29-       32 5 -1.03 -41 (-11 10 -32 33) vol=0.097805 imp:h 1
  30-       33 5 -1.03 -41 (-11 10 -33 34) vol=0.09142 imp:h 1
  31-       34 5 -1.03 -41 (-11 10 -34 35) vol=0.086345 imp:h 1
  32-       35 5 -1.03 -41 (-11 10 -35 36) vol=0.08223 imp:h 1
  33-       36 5 -1.03 -41 (-11 10 -36 37) vol=0.078855 imp:h 1
  34-       37 5 -1.03 -41 (-11 10 -37 38) vol=0.076049 imp:h 1
  35-       38 5 -1.03 -41 (-11 10 -38 39) vol=0.0321835 imp:h 1
  36-       39 5 -1.03 -41 (-11 10 -39) vol=0.0089625 imp:h 1
  37-       40 1 -1 -40 imp:h 1
  38-
  39-       1 rcc 0 0 -10.1 0 0 30 20  $ Phantom boundry
  40-       10 sz 3.546 1.09 $ Choroid/Sclera innerwall
  41-       11 sz 3.546 1.2375 $ Choroid/Sclera outerwall
  42-       20 sz 3.1 .85 $inner cornea
  43-       21 sz 3.1 1.0 $outer cornea
  44-       25 sz 3.3 .75 $ outer lens
  45-       26 sz 2 1  $ inner lens
  46-       27 rcc -0.247 0 4.7655 -0.2 0 1 0.25  $ optic nerve
  47-       30 sz 5.5 2.5 $ Dosimetric spheres
  48-       31 sz 5.7 2.5
  49-       32 sz 5.9 2.5
  50-       33 sz 6.1 2.5
  51-       34 sz 6.3 2.5
  52-       35 sz 6.5 2.5
  53-       36 sz 6.7 2.5
  54-       37 sz 6.9 2.5
  55-       38 sz 7.1 2.5
  56-       39 sz 7.2 2.5
  57-       40 box -10 -10 0.5 20 0 0 0 20 0 0 0 -1.5
  58-       41 px 0
  59-
  60-       mode h n e
  61-       sdef pos -1.5 0 -2 erg d2 vec 0.32 0 1 axs 0.32 0 1 dir 1 ext 0 rad d1 par h
warning.  ext is constant.  in most problems it is a variable.
  62-       phys:h 70
  63-       si1 .5
  64-       si2 0 40.6502 40.7966 44.1944 47.5249 50.6795 53.6850 56.5626 59.3297 62
  65-       c
  66-       sp2 0 0.0509 .0020 0.0587 0.0665 0.0783 0.0902 0.1174 0.1448 0.3914
  67-       c
  68-       m1 1001 -0.11111 8016 -0.8889  $ Water
  69-       m2 1001 -9.6 6012 -19.5 7014 -5.7 8016 -64.6 11000 -0.1 15000 -0.1 16000 -0.3
  70-                17000 -0.1  $ Lens/Cornea (ro=1070kg/m3)
  71-       m3 7014  -9.06E-04   8016  -2.78E-04  $ air
  72-       m4 1001 -10.8 6012 -4.1 7014 -1.1 8016 -83.2 11000 -0.3 16000 -0.1
  73-               17000 -0.4 $ Anterior/Vitreous (ro=1030kg/m3)
  74-       m5 1001 -10.5 6012 -25.6 7014 -2.7 8016 -60.2 11000 -0.1 15000 -0.2 16000 -0.3
  75-               17000 -0.2 19000 -0.2 $Outer eye structure (ro=1030kg/m3)
  76-       m6 15000 -34.7 17000 -56.4 20000 -3.1 12000 -0.62 1001 -1.72
  77-                8016 -2.58 $ Nerve (ro=1040kg/m3)
  78-       F6:H 10 11 12 13 14 20 21 22 23 24 25 26 27 28 29 30 31 32
  79-            33 34 35 36 37 38 39
  80-       FC6 LOOK AT ME
```

```
  81-       nps 300000
  82-       prdmp 2j 1
  83-       c
  84-       c tmesh
  85-       c rmesh11:h flux
  86-       c cora11 -11 11
  87-       c corb11 -11 99i 11
  88-       c corc11 0 99i 30
  89-       c rmesh31:h pedep
  90-       c cora31 -11 11
  91-       c corb31 -11 99i 11
  92-       c corc31 0 99i 30
  93-       c endmd
  94-       c mplot freq 5000 plot ex 20 or 0 0 15
  95-       c      px 0 la 0 1 tal31 col on la 0 0 &
  96-       c      con 1e-4 .2 log
  97-

 warning.  neutron     importances have been set equal to 1.

 warning.  electron    importances have been set equal to 1.

 warning.  use models for the following missing data tables:
  11000.  c
  15000.  c
  11000.  h
  12000.  h
  15000.  h
  16000.  h
  17000.  h
  19000.  h
  20000.  h

 warning.    5 materials had unnormalized fractions. print table 40.


1LAHET physics options:                                                                                    print table 41

 lca    ielas   ipreq  iexisa  ichoic   jcoul  nexite   npidk   noact    icem
 lca        2       1       1      23       1       1       0       1       0

 lcb    flenb(i),i=1,6                                                          ctofe       flim0
 lcb    3.4900E+03  3.4900E+03  2.4900E+03  2.4900E+03  8.0000E+02  8.0000E+02 -1.0000E+00 -1.0000E+00

 lea     ipht     icc  nobalc  nobale   ifbrk  ilvden   ievap   nofis
 lea        1       4       1       0       1       0       0       1

 leb    yzere       bzere       yzero       bzero
 leb    1.5000E+00  8.0000E+00  1.5000E+00  1.0000E+01


 warning.  cross-section file bertin     does not exist.
1cells                                                                                                     print table 60
```

	cell	mat	atom density	gram density	volume	mass	pieces	neutron importance	electron importance	proton importance
1	1	3	5.00973E-05	1.20000E-03	0.00000E+00	0.00000E+00	0	1.0000E+00	1.0000E+00	1.0000E+00
2	2	0	0.00000E+00	0.00000E+00	0.00000E+00	0.00000E+00	0	0.0000E+00	0.0000E+00	0.0000E+00
3	10	2	1.00623E-01	1.07000E+00	6.83139E-01	7.30959E-01	1	1.0000E+00	1.0000E+00	1.0000E+00
4	11	4	1.01510E-01	1.03000E+00	4.50999E-01	4.64529E-01	1	1.0000E+00	1.0000E+00	1.0000E+00
5	12	2	1.00623E-01	1.07000E+00	2.46823E-01	2.64100E-01	1	1.0000E+00	1.0000E+00	1.0000E+00
6	13	4	1.01510E-01	1.03000E+00	4.99775E+00	5.14768E+00	1	1.0000E+00	1.0000E+00	1.0000E+00
7	14	6	2.95831E-02	1.04000E+00	2.00238E-01	2.08248E-01	1	1.0000E+00	1.0000E+00	1.0000E+00
8	15	5	1.02588E-01	1.03000E+00	3.79608E-01	3.90996E-01	1	1.0000E+00	1.0000E+00	1.0000E+00
9	20	5	1.02588E-01	1.03000E+00	1.16600E-01	1.20098E-01	0	1.0000E+00	1.0000E+00	1.0000E+00
10	21	5	1.02588E-01	1.03000E+00	1.05900E-01	1.09077E-01	0	1.0000E+00	1.0000E+00	1.0000E+00
11	22	5	1.02588E-01	1.03000E+00	9.78050E-02	1.00739E-01	0	1.0000E+00	1.0000E+00	1.0000E+00
12	23	5	1.02588E-01	1.03000E+00	9.14200E-02	9.41626E-02	0	1.0000E+00	1.0000E+00	1.0000E+00
13	24	5	1.02588E-01	1.03000E+00	8.63450E-02	8.89354E-02	0	1.0000E+00	1.0000E+00	1.0000E+00
14	25	5	1.02588E-01	1.03000E+00	8.22300E-02	8.46969E-02	0	1.0000E+00	1.0000E+00	1.0000E+00
15	26	5	1.02588E-01	1.03000E+00	7.88550E-02	8.12206E-02	0	1.0000E+00	1.0000E+00	1.0000E+00
16	27	5	1.02588E-01	1.03000E+00	7.60490E-02	7.83305E-02	0	1.0000E+00	1.0000E+00	1.0000E+00
17	28	5	1.02588E-01	1.03000E+00	3.21835E-02	3.31490E-02	0	1.0000E+00	1.0000E+00	1.0000E+00
18	29	5	1.02588E-01	1.03000E+00	8.96250E-03	9.23137E-03	0	1.0000E+00	1.0000E+00	1.0000E+00
19	30	5	1.02588E-01	1.03000E+00	1.16600E-01	1.20098E-01	0	1.0000E+00	1.0000E+00	1.0000E+00
20	31	5	1.02588E-01	1.03000E+00	1.05900E-01	1.09077E-01	0	1.0000E+00	1.0000E+00	1.0000E+00
21	32	5	1.02588E-01	1.03000E+00	9.78050E-02	1.00739E-01	0	1.0000E+00	1.0000E+00	1.0000E+00
22	33	5	1.02588E-01	1.03000E+00	9.14200E-02	9.41626E-02	0	1.0000E+00	1.0000E+00	1.0000E+00
23	34	5	1.02588E-01	1.03000E+00	8.63450E-02	8.89354E-02	0	1.0000E+00	1.0000E+00	1.0000E+00
24	35	5	1.02588E-01	1.03000E+00	8.22300E-02	8.46969E-02	0	1.0000E+00	1.0000E+00	1.0000E+00
25	36	5	1.02588E-01	1.03000E+00	7.88550E-02	8.12206E-02	0	1.0000E+00	1.0000E+00	1.0000E+00
26	37	5	1.02588E-01	1.03000E+00	7.60490E-02	7.83305E-02	0	1.0000E+00	1.0000E+00	1.0000E+00
27	38	5	1.02588E-01	1.03000E+00	3.21835E-02	3.31490E-02	0	1.0000E+00	1.0000E+00	1.0000E+00
28	39	5	1.02588E-01	1.03000E+00	8.96250E-03	9.23137E-03	0	1.0000E+00	1.0000E+00	1.0000E+00
29	40	1	9.98573E-02	1.00000E+00	6.00000E+02	6.00000E+02	0	1.0000E+00	1.0000E+00	1.0000E+00
total					6.08511E+02	6.08806E+02				

random number control 0.830205014835200E+14

minimum source weight = 9.9875E-01 maximum source weight = 1.0000E+00

6 warning messages so far.

1cross-section tables print table 100

table length

tables from file actia

particle-production data for ipt= 31 being expunged from 1001.62c
no particle-production data for ipt= 9 from 1001.62c
1001.62c 5202 1-h-1 at 293.6K from endf-vi.8 njoy99.50 mat 125 12/05/01
particle-production data for ipt= 9 being used from 7014.62c
particle-production data for ipt= 31 being expunged from 7014.62c
particle-production data for ipt= 34 being expunged from 7014.62c
7014.62c 73728 7-n-14 at 293.6K from endf-vi.8 njoy99.50 mat 725 12/05/01

```
 particle-production data for ipt=  9 being used from   8016.62c
 particle-production data for ipt= 31 being expunged from   8016.62c
 particle-production data for ipt= 32 being expunged from   8016.62c
 particle-production data for ipt= 34 being expunged from   8016.62c
   8016.62c  186551  8-o-16 at 293.6K from endf-vi.8 njoy99.50                    mat 825      12/05/01
 no particle-production data for ipt=  9 from  12000.62c
  12000.62c   44838  12-mg-0 at 293.6K from endf/b-vi.8 njoy99.50                 mat1200      12/06/01
 no particle-production data for ipt=  9 from  16000.62c
  16000.62c   68665  16-s-0 at 293.6K from endf/b-vi.8 njoy99.50                  mat1600      12/06/01
 no particle-production data for ipt=  9 from  19000.62c
  19000.62c   26425  19-k-0 at 293.6K from endf/b-vi.8 njoy99.50                  mat1900      12/06/01
 particle-production data for ipt=  9 being used from  20000.62c
 particle-production data for ipt= 31 being expunged from  20000.62c
 particle-production data for ipt= 32 being expunged from  20000.62c
 particle-production data for ipt= 34 being expunged from  20000.62c
  20000.62c   77701  20-ca-0 at 293.6K from endf-vi.8 njoy99.50                  mat2000      12/05/01

                       tables from file rmccs

 no particle-production data for ipt=  9 from   6012.50c
   6012.50c   16126  njoy                                                  (  1306)      79/07/31.

                       tables from file endf66a

 no particle-production data for ipt=  9 from  17000.66c
  17000.66c   25119  17-cl-0 at 293.6K from endf-vi.0 njoy99.50                  mat1700      07/25/01

                       tables from file la150h

   1001.24h   15895  1-h-1 apt la150 njoy 99.20 mcnpx                           mat 125      09/27/00
   6012.24h   51762  6-c-12 apt la150 njoy 99.20 mcnpx                          mat 625      09/27/00
   7014.24h   71369  7-n-14 apt la150 njoy 99.20 mcnpx                          mat 725      09/27/00
   8016.24h   54535  8-o-16 apt la150 njoy 99.20 mcnpx                          mat 825      09/27/00

  total      717916

 maximum photon energy set to   70.0 mev (maximum electron energy)

                       tables from file el03

   1000.03e    2329                                                                        6/6/98
   6000.03e    2333                                                                        6/6/98
   7000.03e    2333                                                                        6/6/98
   8000.03e    2333                                                                        6/6/98
  11000.03e    2337                                                                        6/6/98
  12000.03e    2337                                                                        6/6/98
  15000.03e    2339                                                                        6/6/98
  16000.03e    2339                                                                        6/6/98
  17000.03e    2339                                                                        6/6/98
  19000.03e    2343                                                                        6/6/98
  20000.03e    2343                                                                        6/6/98

1particles and energy limits                                                          print table 101
```

particle type			particle cutoff energy	maximum particle energy	smallest table maximum	largest table maximum	always use table below	always use model above
1	n	neutron	0.0000E+00	1.0000E+37	2.0000E+01	1.5000E+02	0.0000E+00	1.5000E+02
3	e	electron	1.0000E-03	7.0000E+01	7.0000E+01	7.0000E+01	1.0000E+37	1.0000E+37
9	h	proton	1.0000E+00	7.0000E+01	1.5000E+02	1.5000E+02	0.0000E+00	1.5000E+02

The following nuclides use physics models rather than data tables:

11000. c
15000. c
11000. h
12000. h
15000. h
16000. h
17000. h
19000. h
20000. h

decimal words of dynamically allocated storage

general	0	
tallies	3404	
bank	71041	
cross sections	717917	
total	0	= 0 bytes

dump no. 1 on file eye.r nps = 0 coll = 0 ctm = 0.00 nrn = 0

6 warning messages so far.

1problem summary

run terminated when 300000 particle histories were done.

+ 03/24/06 00:58:59

62-MeV SOBP Proton Beam with eye phantom. probid = 03/24/06 00:34:52

neutron creation	tracks	weight (per source particle)	energy	neutron loss	tracks	weight (per source particle)	energy
source	0	0.	0.	escape	2135	7.0624E-03	5.6929E-02
nucl. interaction	0	0.	0.	energy cutoff	0	0.	0.
particle decay	0	0.	0.	time cutoff	0	0.	0.
weight window	0	0.	0.	weight window	0	0.	0.
cell importance	0	0.	0.	cell importance	0	0.	0.

weight cutoff	0	0.	0.
energy importance	0	0.	0.
dxtran	0	0.	0.
forced collisions	0	0.	0.
exp. transform	0	0.	0.
upscattering	0	0.	6.9930E-13
photonuclear	0	0.	0.
(n,xn)	0	0.	0.
prompt fission	0	0.	0.
delayed fission	0	0.	0.
tabular boundary	0	0.	0.
tabular sampling	2135	7.1078E-03	6.2548E-02
total	2135	7.1078E-03	6.2548E-02

weight cutoff	0	0.	0.
energy importance	0	0.	0.
dxtran	0	0.	0.
forced collisions	0	0.	0.
exp. transform	0	0.	0.
downscattering	0	0.	5.0846E-03
capture	0	4.5398E-05	5.3498E-04
loss to (n,xn)	0	0.	0.
loss to fission	0	0.	0.
nucl. interaction	0	0.	0.
particle decay	0	0.	0.
tabular boundary	0	0.	0.
total	2135	7.1078E-03	6.2548E-02

number of neutrons banked	2135
neutron tracks per source particle	7.1167E-03
neutron collisions per source particle	4.0533E-03
total neutron collisions	1216
net multiplication	0.0000E+00 0.0000

average time of (shakes)	
escape	1.8733E+01
capture	8.1203E+00
capture or escape	1.8665E+01
any termination	1.8665E+01

cutoffs	
tco	1.0000E+34
eco	0.0000E+00
wc1	-5.0000E-01
wc2	-2.5000E-01

electron creation	tracks	weight (per source particle)	energy (per source particle)
source	0	0.	0.
nucl. interaction	0	0.	0.
particle decay	0	0.	0.
weight window	0	0.	0.
cell importance	0	0.	0.
weight cutoff	0	0.	0.
energy importance	0	0.	0.
pair production	0	0.	0.
compton recoil	0	0.	0.
photo-electric	0	0.	0.
photon auger	0	0.	0.
electron auger	0	0.	0.
knock-on	0	0.	0.
(gamma,xelectron)	0	0.	0.
total	0	0.0000E+00	0.0000E+00

electron loss	tracks	weight (per source particle)	energy (per source particle)
escape	0	0.	0.
energy cutoff	0	0.	0.
time cutoff	0	0.	0.
weight window	0	0.	0.
cell importance	0	0.	0.
weight cutoff	0	0.	0.
energy importance	0	0.	0.
scattering	0	0.	0.
bremsstrahlung	0	0.	0.
interact or decay	0	0.	0.
total	0	0.0000E+00	0.0000E+00

number of electrons banked	0
electron tracks per source particle	0.0000E+00
electron substeps per source particle	0.0000E+00
total electron substeps	0

cutoffs	
tco	1.0000E+34
eco	1.0000E-03
wc1	0.0000E+00
wc2	0.0000E+00

proton creation	tracks	weight (per source particle)	energy (per source particle)
source	300000	9.9875E-01	5.3862E+01
nucl. interaction	0	0.	0.
particle decay	0	0.	0.
weight window	0	0.	0.
cell importance	0	0.	0.

proton loss	tracks	weight (per source particle)	energy (per source particle)
escape	6359	2.1170E-02	5.3042E-01
energy cutoff	294731	9.8121E-01	9.8045E-01
time cutoff	0	0.	0.
weight window	0	0.	0.
cell importance	0	0.	0.

weight cutoff	0	0.	0.
energy importance	0	0.	0.
dxtran	0	0.	0.
forced collisions	0	0.	0.
exp. transform	0	0.	0.
tabular sampling	12563	4.1824E-02	5.0479E-01
photonuclear	0	0.	0.
elastic recoil	0	0.	0.
(gamma,xgen_chg)	0	0.	0.
total	312563	1.0406E+00	5.4367E+01

weight cutoff	0	0.	0.
energy importance	0	0.	0.
dxtran	0	0.	0.
forced collisions	0	0.	0.
exp. transform	0	0.	0.
multiple scatter	0	0.	5.1008E+01
bremsstrahlung	0	0.	0.
nucl. interaction	0	0.	0.
elastic scatter	0	0.	4.7367E-01
particle decay	0	0.	0.
capture	69	2.2971E-04	3.8699E-03
tabular sampling	11404	3.7966E-02	1.3707E+00
total	312563	1.0406E+00	5.4367E+01

number of particles banked	12563
particle tracks per source particle	1.0419E+00
particle substeps per source particle	1.3381E+02
total particle substeps	40142485

cutoffs

tco	1.0000E+34
eco	1.0000E+00
wc1	0.0000E+00
wc2	0.0000E+00

computer time so far in this run	12.78 minutes
computer time in mcrun	12.71 minutes
source particles per minute	2.3609E+04
random numbers generated	224346274

maximum number ever in bank	3
bank overflows to backup file	0
dynamic storage	0 words, 0 bytes.
most random numbers used was	1518 in history 299794

range of sampled source weights = 9.9875E-01 to 9.9875E-01

lneutron activity in each cell print table 126

	cell	tracks entering	population	collisions	collisions * weight (per history)	number weighted energy	flux weighted energy	average track weight (relative)	average track mfp (cm)
1	1	2347	2135	5	1.6642E-05	2.1495E-01	8.3298E+00	9.9298E-01	1.2439E+04
3	10	264	347	22	7.2968E-05	1.4600E-01	7.7816E+00	9.9517E-01	6.9678E+00
4	11	156	310	28	9.2234E-05	1.2217E-01	7.0264E+00	9.9745E-01	6.6216E+00
5	12	120	192	11	3.6615E-05	3.8341E+00	5.8034E+00	9.9701E-01	6.2613E+00
6	13	275	320	71	2.3333E-04	5.6112E-02	7.3891E+00	9.9529E-01	6.7612E+00
7	14	6	6	0	0.0000E+00	1.1711E+01	1.7904E+01	9.9874E-01	2.0358E+01
8	15	108	107	6	1.9931E-05	7.6182E-01	1.0371E+01	9.9385E-01	7.9312E+00
9	20	33	33	2	6.6583E-06	5.6702E+00	7.9032E+00	9.9874E-01	6.9238E+00
10	21	26	26	1	3.3292E-06	5.8798E+00	8.5499E+00	9.9745E-01	7.1149E+00
11	22	27	27	0	0.0000E+00	7.2597E+00	1.1410E+01	9.9144E-01	7.9806E+00
12	23	22	22	0	0.0000E+00	3.1624E+00	8.2865E+00	9.9368E-01	6.5211E+00
13	24	23	23	1	3.3292E-06	2.9784E+00	6.8342E+00	9.9410E-01	6.2995E+00
14	25	26	26	1	3.3291E-06	4.1606E-02	7.9697E+00	9.9516E-01	6.8103E+00
15	26	24	24	0	0.0000E+00	1.3255E-01	6.1370E+00	9.9809E-01	6.3885E+00
16	27	29	29	0	0.0000E+00	3.8908E+00	7.1281E+00	9.9874E-01	6.6773E+00
17	28	18	18	0	0.0000E+00	6.1887E+00	8.4360E+00	9.9875E-01	7.4059E+00
18	29	8	8	0	0.0000E+00	6.3944E+00	8.6962E+00	9.9875E-01	7.4626E+00
19	30	31	31	2	6.6583E-06	4.1613E+00	7.6853E+00	9.9746E-01	6.8298E+00
20	31	29	29	1	2.9454E-06	4.9797E+00	8.7582E+00	9.9518E-01	7.0724E+00
21	32	25	25	1	3.3292E-06	5.2693E+00	1.1090E+01	9.9874E-01	8.2309E+00
22	33	22	22	0	0.0000E+00	7.4550E+00	9.6635E+00	9.9815E-01	7.9852E+00
23	34	18	18	0	0.0000E+00	7.4445E+00	9.5714E+00	9.9212E-01	8.1862E+00

24	35	19	19	0	0.0000E+00	2.3782E-01	7.2470E+00	9.9871E-01	6.3704E+00
25	36	21	21	3	9.9868E-06	3.0034E-01	6.4765E+00	9.9872E-01	6.0948E+00
26	37	24	24	0	0.0000E+00	2.8104E+00	7.8681E+00	9.9654E-01	6.2616E+00
27	38	12	12	0	0.0000E+00	7.9235E+00	1.3512E+01	9.9433E-01	8.3132E+00
28	39	4	4	0	0.0000E+00	1.0063E+01	1.2674E+01	9.9874E-01	8.5309E+00
29	40	102	1838	1061	3.5050E-03	3.2598E-01	8.0601E+00	9.9174E-01	6.9431E+00
total		3819	5696	1216	4.0162E-03				

1electron activity in each cell print table 126

cell	tracks entering	population	substeps	substeps * weight (per history)	number weighted energy	flux weighted energy	average track weight (relative)	average track mfp (cm)
1	0	0	0	0.0000E+00	0.0000E+00	0.0000E+00	0.0000E+00	0.0000E+00
10	0	0	0	0.0000E+00	0.0000E+00	0.0000E+00	0.0000E+00	0.0000E+00
11	0	0	0	0.0000E+00	0.0000E+00	0.0000E+00	0.0000E+00	0.0000E+00
12	0	0	0	0.0000E+00	0.0000E+00	0.0000E+00	0.0000E+00	0.0000E+00
13	0	0	0	0.0000E+00	0.0000E+00	0.0000E+00	0.0000E+00	0.0000E+00
14	0	0	0	0.0000E+00	0.0000E+00	0.0000E+00	0.0000E+00	0.0000E+00
15	0	0	0	0.0000E+00	0.0000E+00	0.0000E+00	0.0000E+00	0.0000E+00
20	0	0	0	0.0000E+00	0.0000E+00	0.0000E+00	0.0000E+00	0.0000E+00
21	0	0	0	0.0000E+00	0.0000E+00	0.0000E+00	0.0000E+00	0.0000E+00
22	0	0	0	0.0000E+00	0.0000E+00	0.0000E+00	0.0000E+00	0.0000E+00
23	0	0	0	0.0000E+00	0.0000E+00	0.0000E+00	0.0000E+00	0.0000E+00
24	0	0	0	0.0000E+00	0.0000E+00	0.0000E+00	0.0000E+00	0.0000E+00
25	0	0	0	0.0000E+00	0.0000E+00	0.0000E+00	0.0000E+00	0.0000E+00
26	0	0	0	0.0000E+00	0.0000E+00	0.0000E+00	0.0000E+00	0.0000E+00
27	0	0	0	0.0000E+00	0.0000E+00	0.0000E+00	0.0000E+00	0.0000E+00
28	0	0	0	0.0000E+00	0.0000E+00	0.0000E+00	0.0000E+00	0.0000E+00
29	0	0	0	0.0000E+00	0.0000E+00	0.0000E+00	0.0000E+00	0.0000E+00
total	0	0	0	0.0000E+00				

1proton activity in each cell print table 126

cell	tracks entering	population	substeps	substeps * weight (per history)	number weighted energy	flux weighted energy	average track weight (relative)	average track mfp (cm)
1	574517	301131	598841	1.9936E+00	3.4908E+01	3.9187E+01	9.9875E-01	7.8555E+01
10	267277	267895	2277810	7.5832E+00	3.0534E+01	3.2940E+01	9.9875E-01	5.5239E-02
11	251183	252448	4175869	1.3902E+01	2.7798E+01	2.9948E+01	9.9875E-01	4.7884E-02
12	206359	207461	4128366	1.3744E+01	2.3662E+01	2.5543E+01	9.9875E-01	3.4938E-02

6	13	200002	201710	20863360	6.9457E+01	1.5122E+01	1.7326E+01	9.9875E-01	1.8979E-02
7	14	0	0	0	0.0000E+00	0.0000E+00	0.0000E+00	0.0000E+00	0.0000E+00
8	15	1431	1407	35425	1.1794E-01	2.2544E+01	2.5916E+01	9.9875E-01	3.8932E-02
9	20	417	417	14260	4.7474E-02	1.4168E+01	1.6549E+01	9.9875E-01	1.7882E-02
10	21	359	359	14502	4.8279E-02	1.0547E+01	1.2521E+01	9.9875E-01	1.1115E-02
11	22	234	234	11037	3.6744E-02	7.7188E+00	9.4888E+00	9.9875E-01	7.0118E-03
12	23	36	36	1478	4.9205E-03	8.2049E+00	9.8934E+00	9.9875E-01	7.3015E-03
13	24	4	4	178	5.9259E-04	8.0574E+00	8.9279E+00	9.9875E-01	5.5229E-03
14	25	1	1	4	1.3317E-05	1.0593E+01	1.0598E+01	9.9875E-01	6.7575E-03
15	26	0	0	0	0.0000E+00	0.0000E+00	0.0000E+00	0.0000E+00	0.0000E+00
16	27	0	0	0	0.0000E+00	0.0000E+00	0.0000E+00	0.0000E+00	0.0000E+00
17	28	0	0	0	0.0000E+00	0.0000E+00	0.0000E+00	0.0000E+00	0.0000E+00
18	29	0	0	0	0.0000E+00	0.0000E+00	0.0000E+00	0.0000E+00	0.0000E+00
19	30	395	396	5526	1.8397E-02	2.4500E+01	2.7080E+01	9.9875E-01	4.0653E-02
20	31	296	298	4561	1.5184E-02	2.2278E+01	2.4691E+01	9.9875E-01	3.4505E-02
21	32	235	237	4142	1.3789E-02	1.8528E+01	2.0949E+01	9.9875E-01	2.6094E-02
22	33	193	193	4428	1.4742E-02	1.4660E+01	1.6823E+01	9.9875E-01	1.7789E-02
23	34	126	126	3748	1.2478E-02	1.1156E+01	1.2552E+01	9.9875E-01	1.0438E-02
24	35	72	72	2983	9.9309E-03	8.0362E+00	9.1422E+00	9.9875E-01	5.9542E-03
25	36	12	12	508	1.6912E-03	5.2059E+00	5.8367E+00	9.9875E-01	2.6416E-03
26	37	0	0	0	0.0000E+00	0.0000E+00	0.0000E+00	0.0000E+00	0.0000E+00
27	38	0	0	0	0.0000E+00	0.0000E+00	0.0000E+00	0.0000E+00	0.0000E+00
28	39	0	0	0	0.0000E+00	0.0000E+00	0.0000E+00	0.0000E+00	0.0000E+00
29	40	299996	307519	7995459	2.6618E+01	4.3564E+01	4.5417E+01	9.9875E-01	1.0204E-01
total		1803145	1541956	40142485	1.3364E+02				

1tally 6 nps = 300000
+ LOOK AT ME
tally type 6 energy deposition units mev/gram
particle(s): proton

masses

cell:	10	11	12	13	14	20	21
	7.30959E-01	4.64529E-01	2.64100E-01	5.14768E+00	2.08248E-01	1.20098E-01	1.09077E-01
cell:	22	23	24	25	26	27	28
	1.00739E-01	9.41626E-02	8.89354E-02	8.46969E-02	8.12206E-02	7.83305E-02	3.31490E-02
cell:	29	30	31	32	33	34	35
	9.23137E-03	1.20098E-01	1.09077E-01	1.00739E-01	9.41626E-02	8.89354E-02	8.46969E-02
cell:	36	37	38	39			
	8.12206E-02	7.83305E-02	3.31490E-02	9.23137E-03			

cell 10
4.50205E+00 0.0012

cell 11
1.26662E+01 0.0012

cell 12
1.93247E+01 0.0017

cell 13
2.97437E+00 0.0015

cell 14

```
                0.00000E+00 0.0000
cell  20
                7.99208E-02 0.0565
cell  21
                7.15402E-02 0.0616
cell  22
                4.57044E-02 0.0751
cell  23
                6.82166E-03 0.1847
cell  24
                1.01829E-03 0.5696
cell  25
                3.94269E-05 1.0000
cell  26
                0.00000E+00 0.0000
cell  27
                0.00000E+00 0.0000
cell  28
                0.00000E+00 0.0000
cell  29
                0.00000E+00 0.0000
cell  30
                5.24046E-02 0.0583
cell  31
                4.35345E-02 0.0666
cell  32
                3.47745E-02 0.0785
cell  33
                3.16210E-02 0.0852
cell  34
                2.65895E-02 0.1027
cell  35
                1.70463E-02 0.1354
cell  36
                2.35504E-03 0.3205
cell  37
```

```
                0.00000E+00 0.0000

 cell  38
                0.00000E+00 0.0000

 cell  39
                0.00000E+00 0.0000
1analysis of the results in the tally fluctuation chart bin (tfc) for tally   6 with nps =    300000    print table 160


 normed average tally per history  = 4.50205E+00          unnormed average tally per history  = 3.29081E+00
 estimated tally relative error    = 0.0012               estimated variance of the variance  = 0.0000
 relative error from zero tallies  = 0.0006               relative error from nonzero scores  = 0.0011

 number of nonzero history tallies =      266987          efficiency for the nonzero tallies  = 0.8900
 history number of largest  tally  =      158795          largest  unnormalized history tally = 3.18624E+01
 (largest  tally)/(average tally)  = 9.68224E+00          (largest  tally)/(avg nonzero tally)= 8.61677E+00

 (confidence interval shift)/mean  = 0.0000               shifted confidence interval center  = 4.50206E+00


 if the largest  history score sampled so far were to occur on the next history, the tfc bin quantities would change as follows:

      estimated quantities           value at nps           value at nps+1           value(nps+1)/value(nps)-1.

      mean                            4.50205E+00            4.50218E+00                    0.000029
      relative error                  1.24633E-03            1.24663E-03                    0.000237
      variance of the variance        4.38442E-05            4.40825E-05                    0.005435
      shifted center                  4.50206E+00            4.50206E+00                    0.000000
      figure of merit                 5.06629E+04            5.06388E+04                   -0.000474

 the estimated slope of the 200 largest  tallies starting at  2.05104E+01 appears to be decreasing at least exponentially.
 the large score tail of the empirical history score probability density function appears to have no unsampled regions.


 ================================================================================================================================

           results of 10 statistical checks for the estimated answer for the tally fluctuation chart (tfc) bin of tally   6

 tfc bin      --mean--      ---------relative error---------      ----variance of the variance----      --figure of merit--      -pdf-
 behavior     behavior      value    decrease    decrease rate      value    decrease    decrease rate       value     behavior     slope

 desired       random       <0.10       yes       1/sqrt(nps)       <0.10       yes         1/nps          constant     random      >3.00
 observed      random        0.00       yes           yes            0.00       yes          yes           constant     random      10.00
 passed?         yes           yes      yes           yes              yes      yes          yes              yes         yes          yes

 ================================================================================================================================



 this tally meets the statistical criteria used to form confidence intervals: check the tally fluctuation chart to verify.
 the results in other bins associated with this tally may not meet these statistical criteria.
```

```
 estimated asymmetric confidence interval(1,2,3 sigma): 4.4964E+00 to 4.5077E+00; 4.4908E+00 to 4.5133E+00; 4.4852E+00 to 4.5189E+00
 estimated  symmetric confidence interval(1,2,3 sigma): 4.4964E+00 to 4.5077E+00; 4.4908E+00 to 4.5133E+00; 4.4852E+00 to 4.5189E+00

 fom = (histories/minute)*(f(x) signal-to-noise ratio)**2 = (2.361E+04)*( 1.465E+00)**2 = (2.361E+04)*(2.146E+00) = 5.066E+04
1status of the statistical checks used to form confidence intervals for the mean for each tally bin


 tally   result of statistical checks for the tfc bin (the first check not passed is listed) and error magnitude check for all bins

     6   passed the 10 statistical checks for the tally fluctuation chart bin result
         missed all bin error check:    25 tally bins had     8 bins with zeros and     6 bins with relative errors exceeding 0.10


 the 10 statistical checks are only for the tally fluctuation chart bin and do not apply to other tally bins.

 the tally bins with zeros may or may not be correct: compare the source, cutoffs, multipliers, et cetera with the tally bins.

 warning.     1 of the   1 tallies had bins with relative errors greater than recommended.
1tally fluctuation charts

                      tally    6
       nps      mean     error   vov  slope    fom
     16000   4.4957E+00 0.0053 0.0008  6.0   53090
     32000   4.4918E+00 0.0038 0.0004  9.6   51240
     48000   4.5116E+00 0.0031 0.0003 10.0   50741
     64000   4.5040E+00 0.0027 0.0002 10.0   50097
     80000   4.5018E+00 0.0024 0.0002 10.0   49879
     96000   4.5043E+00 0.0022 0.0001 10.0   49990
    112000   4.4998E+00 0.0020 0.0001 10.0   50238
    128000   4.5031E+00 0.0019 0.0001 10.0   50275
    144000   4.5011E+00 0.0018 0.0001 10.0   50446
    160000   4.5027E+00 0.0017 0.0001 10.0   50394
    176000   4.5056E+00 0.0016 0.0001 10.0   50524
    192000   4.5071E+00 0.0016 0.0001 10.0   50571
    208000   4.5072E+00 0.0015 0.0001 10.0   50545
    224000   4.5058E+00 0.0014 0.0001 10.0   50611
    240000   4.5047E+00 0.0014 0.0001 10.0   50630
    256000   4.5040E+00 0.0013 0.0001 10.0   50701
    272000   4.5034E+00 0.0013 0.0000 10.0   50753
    288000   4.5028E+00 0.0013 0.0000 10.0   50716
    300000   4.5020E+00 0.0012 0.0000 10.0   50663

 ********************************************************************************************************************
 dump no.    2 on file eye.r        nps =      300000   coll =       40143701     ctm =   12.71     nrn =      224346274

 tally data written to file eye.m

        7 warning messages so far.


 run terminated when    300000 particle histories were done.

 computer time =   12.78 minutes
```

VITA

Name:	David Bernhardt Oertli
Address:	1126 NE Banner Dr Lee's Summit, MO 64086
Email Address:	David.Oertli@tamu.edu
Education:	B.S., Mechanical Engineering , Colorado State University, 1999 M.S., Health Physics, Texas A&M University, 2006